École polytechnique de Louvain

Impact of humidity on the biomechanical properties of the finger's skin

Author: **Sarah Lallemand**
Supervisors: **Philippe Lefèvre, Benoit Delhaye**
Readers: **Laurent Delannay, Donatien Doumont**
Academic year 2022–2023
Master [120] in Mechanical Engineering

Remerciements

"Je tiens à remercier toutes les personnes sans qui ce travail n'aurait pu être réalisé.

Tout d'abord, le professeur Philippe Lefèvre pour la confiance accordée et l'opportunité donnée de travailler sur un sujet aussi intéressant et Benoit Delhaye pour son encadrement et sa disponibilité tout au long de l'année écoulée. J'aimerais également remercier Donatien Doumont pour son aide et la transmission de ses connnaisances ainsi que sa confiance quant à l'utilisation de son matériel de recherche.

A toute l'équipe du laboratoire de coordonation sensorimoteur de l'Institut des neurosciences (iOns) pour son soutien et sa disponibilité.

Finalement, je tiens à remercier ma famille et mes amis pour leurs encouragements et support moral tout au long de mes études.

Sarah Lallemand"

Abstract

The manipulation of objects is everywhere present in our daily life. Taking the environment into account, our finger's humidity impact such movements. However, the mechanisms underlying our ability to perform the most optimal movements under such conditions are complex. The objective of this work is to calibrate a new moisture evaluator and to focus on the impact of humidity on the main biomechanical properties of the fingerpad such as friction, contact area, and deformations.

Three different initial humidity conditions allowed us to observe the interaction between the moisture level and the normal force, friction, contact area, and deformations. Using the calibrated results from the MeV2 probe, a maximization of friction results from a medium humidity level and a medium contact areas ratio. The normal force also plays an important role during static and dynamic contact, as well as the occlusion phenomenon, increasing the moisture content of the fingerpad. Such results bring a new dimension to the previous research taking online values from the MeV2, which suggests avenues for reflection on the study of object manipulation.

Contents

Nomenclature

α	Pressure coefficient
β	Viscoelastic loss fraction
δ	Indentation of the aspirity into the skin
ν	Poisson's ratio
ϕ	Stick ratio
τ	Interfacial shear strength
τ_0	Intrinsic interfacial shear strength
$a.u.$	Arbitrary Units
A_{gross}	Gross contact area
A_{real}	Real contact area
CF	Coefficient of Friction
E	Young's modulus
F_{ad}	Adhesion component of friction
F_{def}	Deformation component of friction
GF	Grip Force
LF	Load Force
m	Areal load index
$MeV2$	MeV2 output

NF	Normal Force
p	Mean contact pressure
R	Radius of a smooth sphere
$Ratio$	Ratio between A$_{real} and A_{gross}$
TF	Tangential Force

List of Figures

List of Tables

Introduction

The human fingerpad is the central contact point for most tactile interactions, such as object manipulation, texture perception, or haptics exploration. As such, it plays a key role in the sense of touch.

When the hand enters in contact with a surface, multiple biomechanical factors act in order to induce the proper sensory-motor feedback to the brain. Fingerpad's unique biomechanical properties, including visco-elasticity, friction, and deformation characteristics, significantly contribute to our sensory perception because those deformations influence mechanoreceptors' responses. Therefore those responses influence the perception.

However, the brain also has to collect information concerning the environment surrounding the interaction. Previous studies have indicated that changes in humidity levels can significantly alter the interaction between the fingerpad and different surfaces, potentially leading to variations in friction, impacting the grip, and finally perception [17],[4]. Understanding the impact of humidity on the biomechanical properties of the fingerpad would enable us to gain a better understanding of human touch perception. It would also be helpful in developing better models of robotic systems by modeling the interaction between humidity, contact area, and forces.

This master thesis introduces the possibility to characterize the biomechanical properties at any time during prolonged static and dynamic contact with passive subjects. Consequently, the goals of this thesis are multiple. The primary objective is to calibrate a new measurement device called the MeV2 using a previously certified tool called Corneometer. The second objective focus on the impact of humidity on friction, contact area, and deformations.

Chapter 1

State of the art

The fingerpad possesses various biomedical properties that allow us to sense and manipulate an object for a shorter or longer contact time. A brief review of the current state of the art helps contextualize the research. First, the composition of the fingerpad's skin will be described. Then, the definitions of friction and its dependence on the normal force will be discussed. The impact of moisture on the fingerpad and the occlusion phenomenon will also be presented. Finally, the contact area and the deformations of the skin will take part. The contextualization will lead to the description of the objectives of this thesis.

1.1 Composition of the fingerpad's skin

To understand the biomechanical properties of the fingerpads and the impact of moisture on them, we first need to focus on the anatomy of their skin and the localization of the mechanoreceptors involved in perception. Firstly, there are three types of skin; hairy, glabrous (hairless), and mucocutaneous. Unlike many other areas of the body, fingerpads' skin is glabrous. It lacks hair and sebaceous glands, which can interfere with tactile sensation and grip.

As presented in Figure 1.1, the skin's anatomy can be divided into several layers. The outer layer of skin is defined as the epidermis[17]. It is made of four to five layers of epithelial cells. They are, from deep to superficial, the stratum basale, stratum spinosum, stratum granulosum, and stratum corneum. Both the hands and feet have a fifth layer, called the stratum lucidum, located between the stratum corneum and the stratum granulosum[13]. The skin on the finger pads is thus thicker than other areas of the body, providing greater protection against injury and wear.

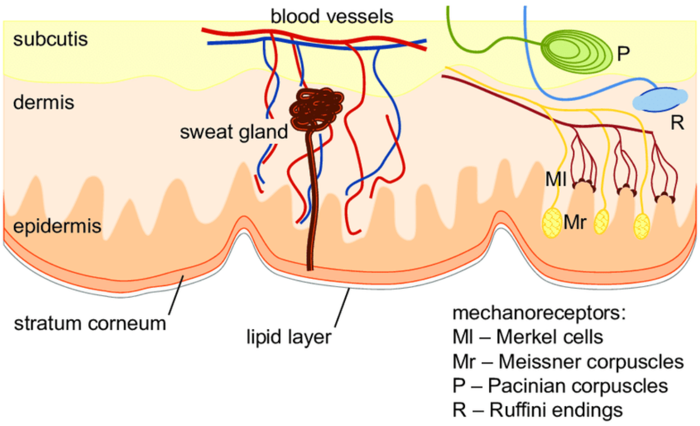

Figure 1.1: Anatomy of the skin of the human fingerpad [15]

Under the epidermis, we can find the dermis which is divided into two layers. The uppermost layer of the dermis called the papillary region is composed of loose areolar connective tissue forming papillae. It contains terminal networks of blood capillaries and nerve endings. The fingerpad skin contains small ridges known as dermal papillae, which help in increasing the roughness of the skin and providing a better grip. The different mechanoreceptors are also located in the dermal region. Merkel cells, which are found at the dermis-epidermis junction, are mechanoreceptors specific to light touch. Meissner's corpuscles are mechanoreceptors that are innervated by nerve fibers located in the dermal papillae and are responsible for the sensation of touch and pressure. They are particularly interesting because of the close connections that they develop with sensory nerve endings. They may contribute to cutaneous nerve development according to Boulais et al [19].

The second layer of the dermis is a thicker layer called the underlying reticular dermis. It is made of densely packed collagen and elastin fibers which provide both strength and elasticity. Other components of the dermis are hair follicles, sebaceous glands, and sweat glands[31]. The fingerpads contain a high density of sweat glands, which help to keep the skin moist and improve grip[26]. Finally, the lowermost layer of the skin is the subcutis.

The fingerpad's skin's unique configuration has several properties which make it well-suited for its specific functions, which include tactile sensation, grip, and dexterity. Those biomechanical properties are still unclear. This thesis thus focuses on the property of the fingerpad's hydration and the impact of humidity on specific parameters such as the coefficient of friction, skin deformation, and the surface of contact.

1.2 Friction and forces

Friction is defined in the Encyclopedia Britannica as the ratio between the tangential force TF resisting the motion of two surfaces in contact and the normal force NF pressing the two surfaces together[8].

$$CF = \frac{TF}{NF} \tag{1.1}$$

However, it exists a difference between static and dynamic coefficients. Static friction represents the frictional force applied while the object remains static. Dynamic friction slows down the object's movement by resisting the force applied. Both coefficients of friction are influenced by the normal force as Coulomb friction law states (equation 1.1), but also by the properties of the object's surface such as its roughness and hardness as demonstrated by Adams et al [18]. Figure 1.2 shows that the friction of the fingerpad decreases with increasing roughness of the countersurface due to a reduction in the capillarity forces. Koris A. defines a capillarity force as a force that generates movement of a liquid along the surface of a solid caused by the attraction of molecules of the liquid to the molecules of the solid [2].

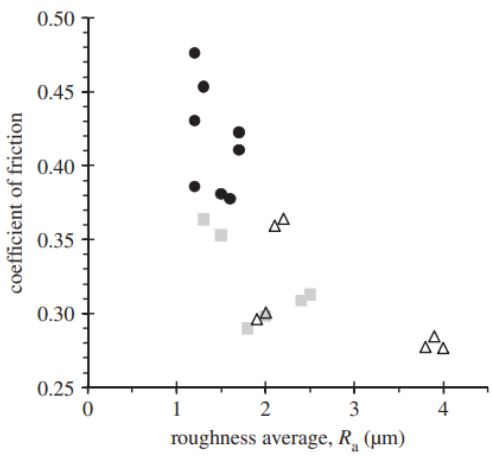

Figure 1.2: The dynamic coefficient of friction for different types of paper as a function of surface roughness (Triangles: uncoated; Squares: coated mechanical; and Circles: woodfree-coated).[18]

When we work with active manipulation and oscillations, the force applied by the hand when grasping and holding an object directly impacts the coefficient of friction, this is the grip force [1]. In fact, when moving a hand-held object, the grip force is automatically modulated based on fluctuations in the load force that depend on the weight and the acceleration of the object. For example, going from a downward to an upward movement with an object implies a greater load force, and thus a greater grip force to avoid slippage. Accidental slips can thus be avoided because the grip force exceeds the minimal force required to prevent slip, called the slip force, by a safety margin determined by the skin-object friction[21]. The grip force should counteract the gravitational force and inertial components of the tangential load force.

$$Margin = |\underbrace{GF * CF}_{LF_{min}} - LF| \tag{1.2}$$

1.3 Impact of moisture

In addition to the relation between the coefficient of friction and the grip force, studies also found that the skin's friction of the fingerpad increases in the presence of a certain amount of water and decreases during a drying period. In 1975, Adelman et al. observed that people sweat on their palms and feet in response to stressful situations and exercise which would increase the resistance of the skin, the tactile sensitivity, and as well as the coefficient of static friction[23]. However, when the hand or footpad is in constant contact with the surface, a large amount of sweat also builds up and a layer of water forms, which results in a decrease of the coefficient of static friction, and slippage could occur. Thus, at a very wet stage, friction could decrease due to the presence of a thin layer of water between the skin and the object.

In 2008 and 2009, during precision grip manipulations, a prototype was created to record the evolution of the moisture level and the coefficient of friction at any time during the dexterous manipulation. To quantify the moisture level, André and al. used a resistor in parallel with a capacitor to use the principles of capacitance and conductance as it is shown in Figure 1.3 [30]. The capacitor is charged and discharged at a frequency dependent on the resistance of both the finger and the probe. The value of both components is influenced by the water content of the skin. A higher frequency signal represents an increased water content at the skin surface. As the sensitivity of the conductance method is poor for low levels of hydration in opposition to the resistance model, both models are complementary. Moreover, two different levels of normal forces applied were compared, and it was found that it would only introduce a moderate offset in the measurements of the moisture level when we compare this new method with an already-known measurement method: the Corneometer.

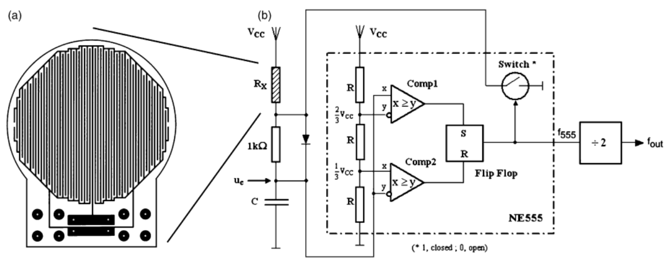

Figure 1.3: Network of electrodes that constitutes the probe of André et. al's Moisture Evaluator and its electronic circuit measuring the conductance.[30]

This experiment revealed a significant influence of moisture on friction for net forces below 3.5N[28]. The friction reached a maximum for an intermediate level of humidity shown by a bell-shaped curve of the coefficient of friction (Figure 1.4). However, it was not visible for a force larger than 3.5N. Indeed, humidity has less and less impact on friction for high forces. Finally, they show a negative power function between the coefficient of friction and the normal force for the same level of moisture, leading to a decrease in friction when the force is increasing[28]. A relevant interaction exists then between those three parameters friction, moisture, and net force, except for a very wet state.

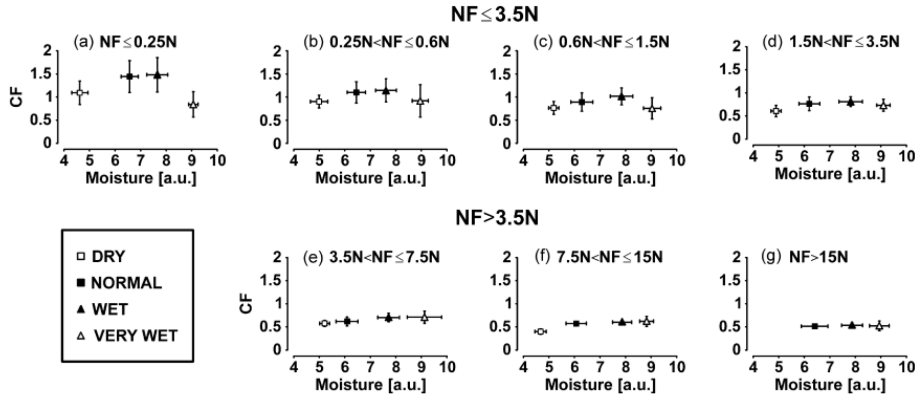

Figure 1.4: Relationship between the CF and moisture for different ranges of Normal Force from below 0.25 N to above 15 N. Each data point corresponds to the mean CF and moisture content for the specific moisture ranges recalled in the legend.[28]

As said before, the experimental data of André et al. [29] were calibrated on results obtained with the Corneometer. This Corneometer is a tool used to measure the hydration level of a dielectric medium, here the skin's stratum corneumn[11]. With increasing hydration, its dielectric properties change. The measurement is based on the fact that water has a higher dielectric constant than most other substances. So, it works by measuring the electrical capacitance of the skin, which is related to its water content.

Figure 1.5: The Corneometer is the worldwide most used probe to measure skin hydration.[11]

The Corneometer (represented in Figure 3.1) consists in a probe placed onto the skin's surface, which conducts a small, high-frequency electrical current. This current passes through the stratum corneum and into the underlying tissues, where it encounters resistance from the water molecules present in the skin. The Corneometer then measures the amount of current that is absorbed by the skin and uses this information to calculate the skin's hydration levels[12]. The results of the Corneometer are expressed as arbitrary units that vary between 0 and 120, with higher numbers indicating greater hydration levels. This tool is often used to assess the efficacy of moisturizing products, as it will be the case in our research. However, the values obtained depend on the surface of the finger in contact with the probe, which can vary a lot since the probe is small and the finger is free to move. Additionally, this tool records point values, such that it does not depend on the duration of the contact and thus does not take into account the phenomenon called occlusion. It also does not control the normal force and only measures moisture at a fixed arbitrary normal force applied.

1.4 Occlusion phenomenon

In static contact with a surface, skin surface occlusion by the counter body results in moisture accumulation. This phenomenon happens when the skin deforms and flattens against the surface (Figure 1.6). It prevents the evaporation of moisture from the skin surface leading to an increase both in the bulk moisture level of the stratum corneum and also at the interface[26]. The occlusion phenomenon is more important as the number density of sweat pores is high. Hydration of the skin, due to occlusion, would enhance the finger's viscous properties which would augment the adhesion effect. Since static contact occurs often in the daily life of a person and is not much understood, a deeper analysis of its impact on friction, contact area, and moisture regulation is required.

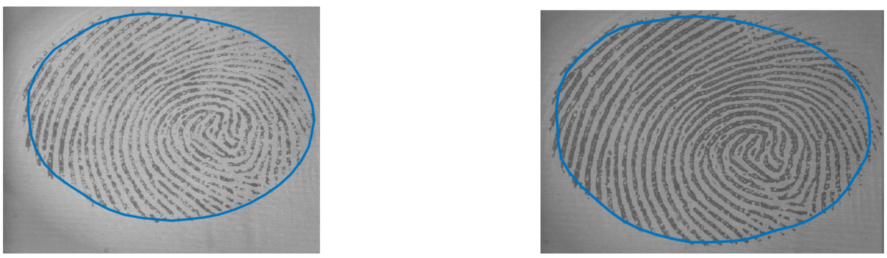

Figure 1.6: Fingerpad images after 3 seconds of contact (left) and after 30 seconds of static contact (right).

Previous research focused on the impact of the duration of the occlusion and revealed an adaptation of the moisture level in order to maximize the coefficient of friction. Indeed, Figure 1.7 shows that the moisture arising from occlusion and external wetting tends to a path-independent steady-state volume fraction that corresponds to the maximum value of the friction, thus ensuring optimal grip[27]. This means that starting from a very wet state or very dry state tends to end with the same value of the coefficient of friction after a certain amount of time. The friction starts very low for a very wet state since there is the presence of a thin layer of water between the surface of the object and the finger, but with time, evaporation occurs to reach a better coefficient of friction. Looking at the previous papers, this time was set to 30 seconds as it represents the start of stabilization of friction.

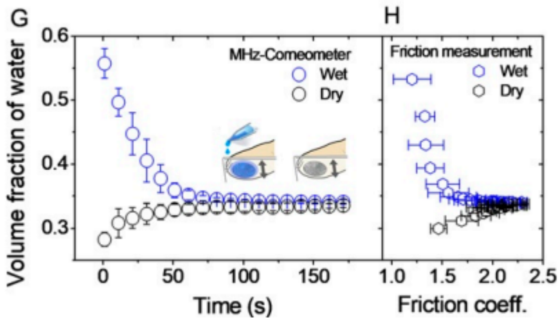

Figure 1.7: Left: The hydration level as measured using a Corneometer for an initially "wet" and "dry" fingerpad; regardless of the initial wet or dry conditions, the volume fraction of the moisture converges to an asymptotic value. Right: Relationship between frictional force and the hydration level showing that the maximum friction is achieved at the converged hydration state.[27]

1.5 Contact area and deformation during sliding contact

Friction also depends on the properties of the surface of the object and the glabrous skin of the fingertips. Adams et al. decomposed it by a two-term model including adhesion and a deformation term[18]. The deformation mechanism represents the amount of work dissipated due to viscoelastic hysteresis times the sliding displacement[16].

$$F_{def} = \frac{3}{16}\beta\frac{\delta}{a} NF, \tag{1.3}$$

where β represents the viscoelastic loss fraction and δ the indentation of the aspirity into the skin. The viscoelastic loss was observed close to 0.31 for dry skin and 0.79 for wet skin with $\beta = \pi \tan \delta$ [32].

The adhesion mechanism is expressed as:

$$F_{ad} = \tau A_{real} \tag{1.4}$$

with F the frictional force, τ the interfacial shear strength, and A the real area of contact. The parameter τ depends on the contact pressure p and, thus, on the normal force applied.

$$\tau = \tau_0 + \alpha p, \tag{1.5}$$

where τ_0 is the intrinsic interfacial shear strength, α is the pressure coefficient and p is the mean contact pressure calculated as the ratio between the normal force and the real contact area. When a movement started, the center of pressure moved slowly and the tangential force increased monotonically. However, after slippage, the slope of the displacement of the center of pressure increased a lot while the force remained the same[28]. That's how slippage is detected.

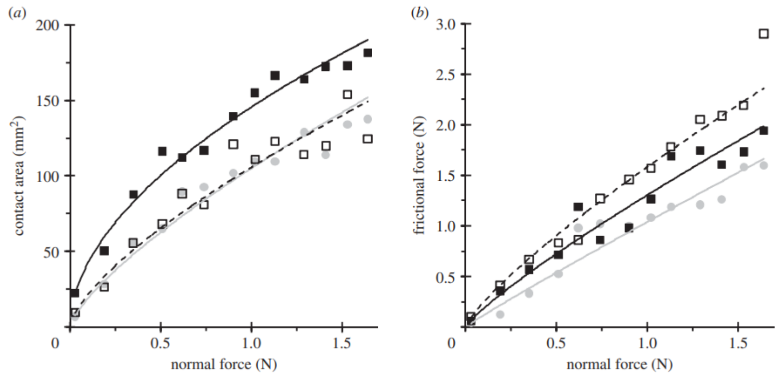

Figure 1.8: The relationship between (a) the contact area and (b) the dynamic frictional force of individual fingerpads as a function of the applied normal force, for three different fingers held flat against an acrylic sheet. Index finger, squares; middle finger, circles, and thumb, squares. The lines are the best fits of equation 1.6 [18]

The area of contact then plays a massive role in friction. Indeed, the increase of friction during occlusion can be ascribed to an increase in the real contact area, resulting from the specific effects of water plasticization on the stratum corneum. The deformation of the plasticized asperities induces an increase in the contact area responsible for a larger coefficient of friction in the wet state. This is due to the topographical features of the skin that are flattened under typical sliding contact pressures. The fingerpad then behaves as a smooth body[17]. However, as shown in Figure 1.8, this area varies also with normal force following a power law that we can write as[18]:

$$A_{real} = kNF^m = \pi[\frac{3R(1-\nu^2)}{4E}]^{2/3}NF^{2/3} \tag{1.6}$$

where R is the radius of a smooth sphere (the fingerpad), E and ν are Young's modulus and Poisson's ratio of the deformable body. Friction then increases with the absorption of moisture due to the plasticization that reduces Young's modulus. In addition, the contact area decreases during tangential loading[6]. The entire contact area slipped when the tangential force is maximum[29]. This last phenomenon called the peeling mechanism was studied by Delhaye et al. It would be due to the compression or expansion of the tissue in contact with the glass and depends on the direction of movement. For radial and ulnar directions, peeling occurs on the side of the direction of motion. The short axis of the oval shape was strongly reduced. Moreover, it was shown that the skin gets stiffer when the tangential force increases, and thus Young's modulus of the fingerpad increases[4].

Sliding contact induces slippage which starts with a 'stick-to-slip' behavior. It means that the 'incipient' (or partial) slips start at the periphery of the contact and grow toward the center called the 'stuck' area. That phenomenon ends with the whole contact slipping. The propagation of a progressive strain wave from the periphery to the center of the contact area with the largest strain values located at the periphery of the contact was observed. It was compressive ahead of the stuck area and tensile behind it[6]. The compressive part is dominant in the ulnar and radial displacement.

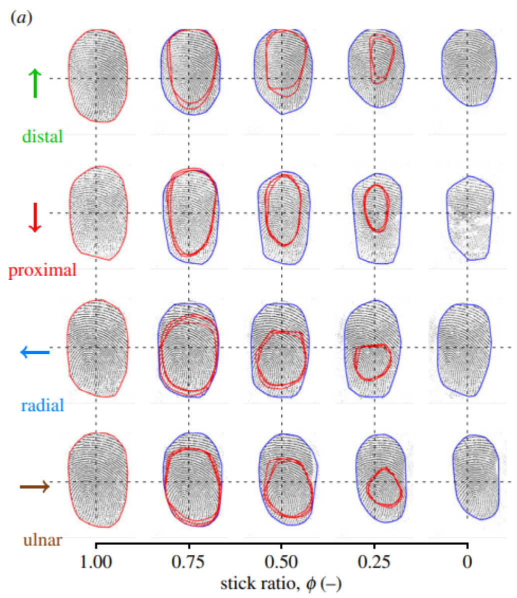

Figure 1.9: Evolution of the stuck area for stick ratios of 1, 0.75, 0.5, 0.25, and 0 for each direction. Blue contours surround the contact area, red contours represent the stuck area.[4]

During a partial-slip phase, the contact area decreased, and the stick area monotonically decreased to zero. Then, that area stabilized to a constant value. Right after the full slip, the tangential force continues to increase for a moment, while the coefficient of dynamic friction decreases as the normal force increases[4]. The partial slip was observed and quantified by the stick ratio, which typically reached a minimum when the constraints were maximal, which happened at the maximum load force or the minimum grip force overload force ratio. When the stick ratio decreases, the strain propagates toward the center (Figure 1.9). The minimum value for the stick ratio within an oscillation was low for low levels of grip force and tended to 1 for high levels of grip force[5]. A linear decrease in the stick ratio exists as a function of the tangential force. However, to produce partial slip, a minimal force is required due to the presence of an intrinsic interfacial shear strength. This minimal force increases with normal force. Moreover, the parts of the fingerprint ridges aligned with the direction of motion have a tendency to slip earlier.

1.6 Aim of the work

The objective of this master thesis is to investigate the influence of humidity on finger-pad deformations and its impact on contact interactions. To achieve this, a specialized probe called MeV2 has been developed to monitor the online moisture and capture images of the contact surface. The primary goal is to calibrate the MeV2 and assess its sensitivity to various biomechanical factors such as normal force, tangential force, friction, and other relevant outputs.

This research will, at first, focus on analyzing the interaction of humidity with the tangential forces, the tension in the MeV2, the contact area, the applied normal force, and the skin's deformations. Furthermore, the study aims to explore the phenomenon of occlusion during static contact. Specifically, we aim to understand how this phenomenon evolves over time on the fingertip and determine the humidity level at which the coefficient of friction reaches its maximum. Additionally, we seek to investigate how this phenomenon regulates the moisture level and to understand how humidity can be adjusted as needed. To accomplish these goals, we will closely examine the temporal evolution of moisture and changes in the contact area.

Chapter 2

Method

This section encompasses the development of the methodology and experimental protocol employed in our research. The first part centers on the subjects involved and the apparatus utilized. Various tests conducted to refine the final protocol are also explained. In a second time, a comprehensive description of the final protocol is provided. Lastly, we expound on the methodology employed for data and image processing.

2.1 Subjects

16 healthy volunteers gave their written informed consent to participate in the experiment. They were aged from 21 to 57 years. 10 women and 6 men formed the panel of subjects. The local ethics committee approved the study.

2.2 Apparatus

The probe comprises a comb-shaped network of 10µm-width ITO isolated by a 2µm-thickness layer of PMMA. Those two materials enable the obtention of an almost completely transparent probe allowing the capture of images of the fingerpad at the same time as the capacitance of the skin in contact. The geometry of the network is designed to have measurements at three different locations across the surface. Those locations are called patches (Figure 2.1).

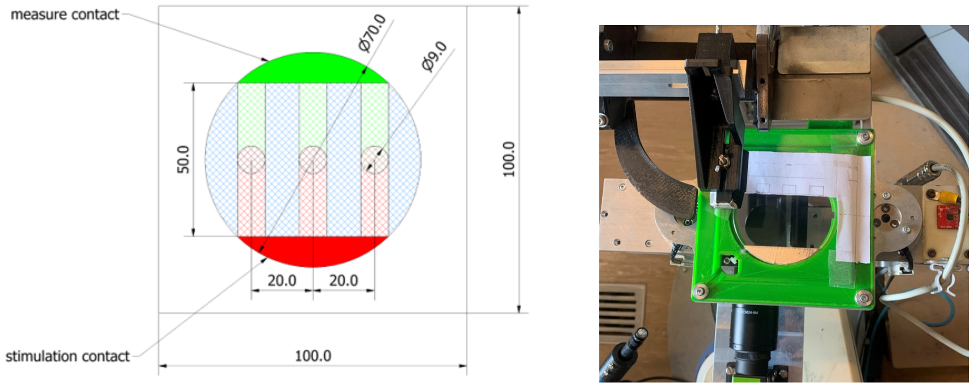

Figure 2.1: Transparent glass probe with the three patches represented by the small circles in the middle of the annotated plan (on the left). The final probe (on the right) lies on the robot end-effector.

The probe was installed on the head of a robotic platform in order to control the movement. Indeed, a scara robot was used to apply a constant velocity movement. It is an industrial four-axis robot (DENSO HS4535G) that can translate in three orthogonal directions. Its position is servo-controlled with a position resolution of 15 µm by a factory controller at a frequency of 1 kHz, as described in Delhaye et al. paper[4]. The displacement velocity was set at 5 [mm/s]. In addition, the normal force applied was also controlled by a servo-motor. Two force/torque sensors (ATI mini40), which measure the normal and tangential forces that are applied to the fingertip along each direction, allow the motor to send the proper amount of charge to the finger and adjust it to keep a constant normal force. All the components are represented in Figure 2.2.

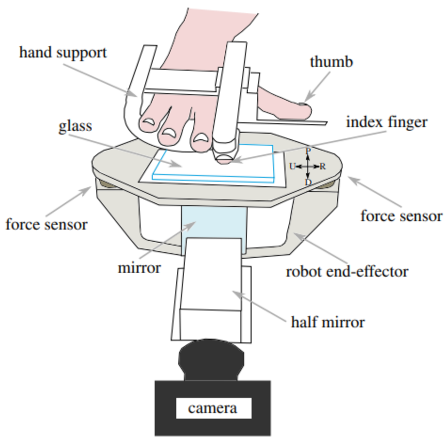

(a) Detailed schematic [4]

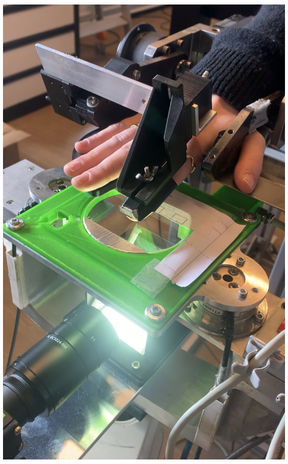

(b) Pictures of the real apparatus with the subject's hand

Figure 2.2: Apparatus used for the experiment. The subject's hand is resting on the hand support, with the right index finger fixed. The end-effector of the robot, with the transparent glass probe, translates precisely in any direction. The two force/torque transducers are also located on the end-effector. The imaging system comprises a camera, a half mirror, and a full mirror under the probe.

The subject's right index finger was placed in a support that ensured precise guiding of the nail position and full relaxation of the hand. This was important in order to have a completely passive experiment.

A camera fixed on the ground could record images of the fingertip contact zone through the glass plate at high frequency and high resolution (JAI GO-5000-PMCL, 2560x2048 pixels). Using a light reflection system, a high contrast between fingerprint ridges and valleys was achieved [6]. Regions in contact with the glass plate appear much darker in the images because the light is scattered and transmitted to the finger. Coaxial illumination, however, produces lower contrast images than prism-based frustrated reflection since the background inter-ridge surfaces reflect significant light, but it has the advantage of giving images that do not require aspect-ratio correction[24].

In order to validate the right way to reach the largest range of humidity, preliminary experimentations were done with the Corneometer (Figure 2.3a). Ehter shows that it is difficult to increase the moisture level after its application. This leads to using it in the final set of measurements. Moreover, it was shown that water is allowed to reach a high level of humidity but then the finger's skin dries fast. It was then important to apply water just before starting the measurements and not wait too much. The time of application of water was also defined based on some personal experiments. It was decided to tap on a towel all soaked in water for an entire minute before each set and to recall the tapping every 5 trials as it was suggested by Tomlinson et al. during their research about friction[25]. It was also important to clean hands with soap 10 minutes before starting the experiment to avoid a greasy layer on the skin proper to the subject that would bias the results.

On the probe, different levels of normal forces were tried in order to select the best and most pertinent values. Figure 2.3b demonstrates that voltage does not increase linearly with the normal force applied. This observation coincides with the previous papers saying that some interactions were not visible under normal forces higher than 3.5N. The 3 different levels of force are applied in a different order for every subject.

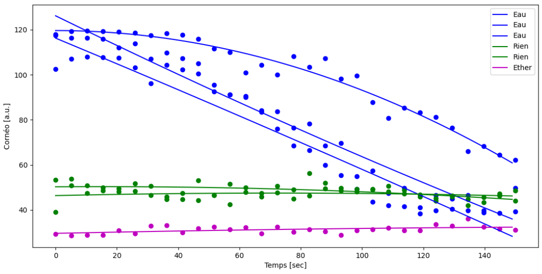

(a) Trials of different humidity states. Blue represents the action of a droplet of water on the fingerpad before the trial, purple stands for the action of ether on the fingerpad before the trial, and the green represents the normal state.

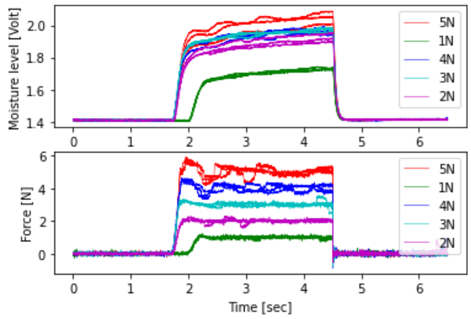

(b) Impact of a large range of normal force on moisture: red for 5N, dark blue for 4N, light blue for 3N, purple for 2N, and green for 1N.

Figure 2.3: Experiments to determine the protocol

2.3 Experimental procedure

Since the main goal of this research is to calibrate the new probe and focus on the occlusion phenomenon, a protocol with 3 main conditions was designed: calibration, slide with occlusion, and slide without occlusion. Each condition was tested with three moisture states (normal, moist, and dry). Within each condition, 15 trials were performed (5 rep x 3 NF). The whole protocol thus involved 135 trials (3 states x3 cond x 15 trials).

The first condition called the "calibration" is described by 20-second long trials composed of 3 seconds of static contact on the transparent probe before the extract of the robot followed by taking a value with the corneometer.

The second condition called the "occlusion" is described by 60-second long trials composed of 30 seconds of static contact, a displacement of 42mm from the right patch to the left patch without stopping on the middle one, and 3 seconds of relaxation before taking a value with the corneometer.

The third and final condition, "slide" is similar to the second condition but with a shorter static contact on the first patch. Indeed, the displacement started only 3 seconds after the start of the force's application. Each trial was 30 seconds long.

Each condition was used for the 3 different moisture states: normal, wet, and dry. To reach the humid state, one minute of tapping on a towel all soaked in water was done before starting each condition. As said before, a recall of this procedure, but for only 30 seconds, was realized every 5 trials which corresponds to a change of normal force. As far as it concerns the dry state, a droplet was applied on the finger every 5 seconds to let it dry on the skin, for a total of one minute before each condition. Similarly to the humid state, a recall of 30 seconds was done after every 5 trials. Nothing was used for the normal state.

To make sure that any residual humidity stayed on the probe, it was cleaned after every trial as well as the patch of the Corneometer.

The subject was seated on a long chair on the left of the apparatus. This means that the dominant hand was not taken into account in the choice of the index finger used for the experiment. The hand had to be relaxed which was only possible if the initial position, height, and depth of the finger were set for each individual subject.

2.4 Data processing

Tangential forces, normal force, and voltage have been recorded with the MeV2 probe at a sampling rate of 1 kHz. To make sure that the images and the MeV2 were both set and well synchronized, we introduced a delay of 4 seconds before the loading phase and ended when the loading was over.

Let TF_x be the tangential force in x direction and TF_y be the tangential force in y direction, the total tangential force, expressed in Newton, is computed as:

$$TF = \sqrt{TF_x^2 + TF_y^2} \tag{2.1}$$

The arithmetic means of the normal force [N] and voltage [V] of each trial are computed over the last second on each measurement patch of the MeV2. Practically, for the "calibration" condition, NF_{mean} and $MeV2_{mean}$ are computed between t=6sec and 7sec. For the "occlusion" condition, NF_{mean} and $MeV2_{mean}$ are computed between t=32.5sec and 33.5sec for the first patch (right), and between t=42.5sec and 43.5sec for the last patch (left). Concerning the "slide" condition, NF_{mean} and $MeV2_{mean}$ are computed between t=6sec and 7sec for the first patch (right), and between t=16sec and 17sec for the last patch (left).

The arithmetic mean of the tangential force [N] is computed during the displacement. To make sure that full slippage is reached and that relaxation is not happening yet, F_{mean} is computed between t=37.5sec and 20.5sec in the "occlusion" condition, and between t=11sec and 14sec in the "slide" condition.

Moisture is recorded with the Corneometer after each trial. This value is expressed in arbitrary units from 0 to 120[a.u.] (section 1.3). A very dry state is represented by a value of $\pm 20[a.u.]$, while a very wet set is $\pm 120[a.u.]$.

2.4.1 Images processing

The images are given in '.avi' files and are recorded at a sampling rate of 50Hz. Those files were so heavy that it was required to compress them into '.mp4' files and to jump some frames. Indeed, during the first 3 seconds of the loading phase, during the movement, and during the relaxation period, all the frames are important. Nevertheless, when the contact is static, a lower acquisition frequency can be used (2Hz). Once the compression is done, 724 frames are obtained for one trial in the "occlusion" condition, 670 frames for the "slide", and 150 frames for the "calibration".

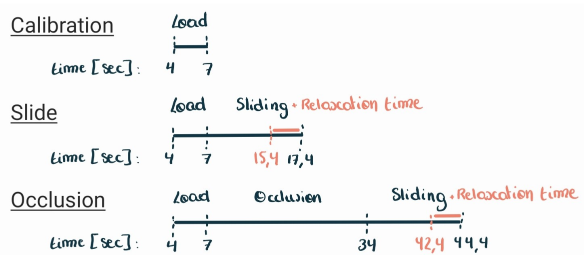

Figure 2.4: Segmentation of each trial depending on the condition.

Since such an amount is very time-consuming, a focus is done on the most pertinent images. The trial can be divided into 3 main parts which are: the 'loading' phase, corresponding to the first 3 seconds (150 frames at 50 Hz) of loading similar in every condition, the 'occlusion' phase, corresponding to the 27 seconds (54frames at 2 Hz) of extra static loading only present in the "occlusion" condition, and the 'slide' phase, corresponding to the 10.4 seconds (520 frames at 50 Hz) of sliding and relaxation include in the "slide" and "occlusion" conditions. This segmentation is illustrated in figure 2.4. To analyze the evolution of the contact area during the occlusion phenomenon, the last frame of the 'loading' phase and all of the images during the 'occlusion' phase are kept. In addition, as the deformations are also studied, the 150 first frames of the 'slide' phase are kept. The total amount of frames is reduced to a maximum of 205 for an "occlusion" trial and 151 for a "slide" trial.

The contact area can have multiple meanings. The gross area, A_{gross}, corresponds to the overall area with the elliptical shape that represents the entire perimeter of the contact. The real contact area, A_{real}, is an approximation of the most precise contact area to characterize. It can be computed as the sum of small segments of the ridges that are in contact with the glass that eventually connects to form A_{ridge}, the contact area excluding the interstitial spaces between the ridges[24].

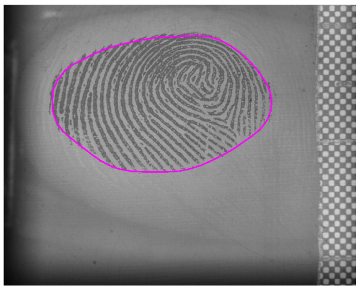

Figure 2.5: Images of the fingerpad with the contour of the gross contact area.

The first step in image processing is to extract the gross area for every frame of all the subjects. As described in Delhaye et al. procedure [5], the contact area contour was manually extracted for a small subset of frames (15 frames by humidity condition, for a total of 45/subject). In the second phase, relevant features for segmentation, explained by Sankaran [3], are calculated and used as inputs for a machine learning algorithm. Specifically, a MATLAB classification tree is employed, which is trained using manually segmented data. This trained model is then utilized to extract the gross contact area from the entire sequence of frames. This area is represented by the purple oval shown in Figure 2.5.

The second step allows us to extract the ratio between the real area and the gross area. The images previously extracted from the model are filtered. Everything outside the mask is avoided and not further used, such that we only keep everything inside the gross area. To compute the real area, 'imbinarize(I,T)' creates a binary image (Figure 2.6) from the inside of the gross area by replacing all values above a certain threshold T by 1 and the others by 0 [10]. The threshold is computed using Otsu's method, which separates each point of the image into two classes, foreground and background, by minimizing their intraclass variance[20]. This value is valid only when the contrast is quite high and thus when the effectiveness metric of the 'graytresh' method is higher than 0.7. Below 0.7, a correction was necessary.

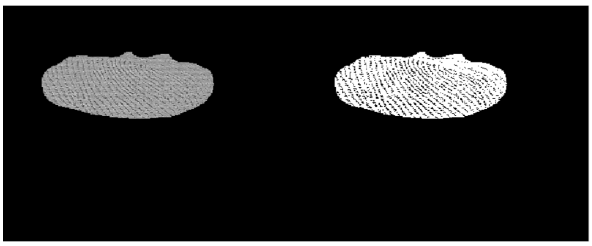

Figure 2.6: Comparison between the gross area before binarization on the left, with the image after binarization on the right. The black part inside the right image represents the real area.

The optical flow technique, described by Benoit et al. [4], is used to obtain the displacement vector field. For each feature, selected as trackers from frame to frame in the contact area, a relative displacement vector between the finger and the glass was obtained by subtracting the stimulus displacement from the feature displacement. Indeed, a Delaunay triangulation of the feature points sampled in the first frame was computed and, for each triangle, displacement field gradients were derived and attributed to the center of the triangle[6]. The displacement gradient in the contact area allows us to compute the Green-Lagrange strains:

$$E_{11} = \frac{\delta u_1}{\delta X_1} + \frac{1}{2}[(\frac{\delta u_1}{\delta X_1})^2 + (\frac{\delta u_2}{\delta X_1})^2 + (\frac{\delta u_3}{\delta X_1})^2] \tag{2.2}$$

$$E_{22} = \frac{\delta u_2}{\delta X_2} + \frac{1}{2}[(\frac{\delta u_1}{\delta X_2})^2 + (\frac{\delta u_2}{\delta X_2})^2 + (\frac{\delta u_3}{\delta X_2})^2] \tag{2.3}$$

$$E_{12} = \frac{1}{2}[\frac{\delta u_1}{\delta X_2} + \frac{\delta u_2}{\delta X_1} + \frac{\delta u_1}{\delta X_1}\frac{\delta u_1}{\delta X_2} + \frac{\delta u_2}{\delta X_1}\frac{\delta u_2}{\delta X_2} + \frac{\delta u_3}{\delta X_1}\frac{\delta u_3}{\delta X_2}] \tag{2.4}$$

The components E11, E22 correspond to ϵ_{xx} and ϵ_{yy}, and are termed normal or axial strains and E12 corresponds to ϵ_{xy}, and is called shear strain[14]. u_1 corresponds to the displacements along x while u_2 represents the displacements along y. There is no displacement along z so u_3 is null.

It was then possible to compute the maximal shear stress for each frame which gave a numerical value to work with. The maximal shear stress was obtained with the use of Mohr's circle. Indeed, the maximal shear stress is the radius of the circle which can be estimated as the difference between the two axial strains divided by two. Its evolution through the different frames reflected the accuracy of the trial. If there was not a clear peak before the relaxation of the shear stress, an error in the image processing did happen and the trial could not be used.

2.4.2 Linear regression

Simple linear regression is a statistical model that estimates the relationship between a dependent variable and other independent variables. Simple linear regression is used to prove how strong the relationship is between two variables. Regression models describe the relationship between variables by fitting a line to the observed data[22] that can be used to make predictions or understand the relationship between the variables. The function 'numpy.polyfit', used during the research, employs the ordinary least squares method (Figure 2.7) which minimizes the sum of squared errors (SSE) between the predicted values on the line and the actual values in the dataset[9].

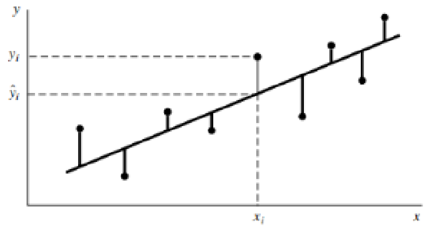

Figure 2.7: Fitting a straight line through a set of data points using the ordinary least squares method [9]

2.4.3 Statistical approach

To validate the multiple observations some statistical tests have been carried out. To estimate the linear relationship, Pearson's correlation coefficient R is computed. This coefficient varies between -1 and 1, 0 meaning that no correlation exists. A positive sign represents an increasing line, while a negative coefficient means that the y-values decrease when the x-values increase. In addition, the probability of an uncorrelated and normally distributed system possessing a similar Pearson's correlation coefficient is estimated through a p-value, using the traditional 0.05 to determine the statistical significance. A value smaller than 0.05 means a significant correlation.

To analyze the difference between the means of more than two groups of samples, an ANOVA test is used. A one-way ANOVA uses one independent variable, while a two-way ANOVA uses two independent variables. The independent variable is categorizable while the dependent variable is quantitative. The null hypothesis (H_0) of ANOVA is that there is no difference among group means. The alternative hypothesis (H_i) is that at least one group differs significantly from the overall mean of the dependent variable [7]. If any of the group means is significantly different from the overall mean (p-value<<0.005), then the null hypothesis is rejected.

Representation with a boxplot allows the highlighting of some outliers but also of a mean value that would be used for further statistical tests. Comparisons between different conditions are also made using Boxplot.

Chapter 3

Results

This section is divided into several parts corresponding to the various data that have been analyzed in the same order as the one followed during the research. First of all, the Corneometer values are presented. Data extracted from the MeV2 are then introduced before reviewing results obtained on the basis of the acquired images.

As the objective is to show the impact of moisture on the different biomechanical properties of the fingerpad, its influence on each parameter was investigated. Different correlations between moisture measurements and other parameters were performed in multiple sections. The calibration between the Corneometer and MeV2 methods is also described in the MeV2 section.

A similar legend is used for every graph using the MeV2. Indeed, to represent the trials under a normal force of 1N, the royal blue color from MATPLOTLIB is used, when orange and green are respectively used for a normal force of 2N and 5N. A different marker is also used for each humidity level. The crosses represent a 'normal' moisture, the dots represent a 'humid' moisture, and the squares represent a 'dry' moisture.

Finally, only one subject is shown when the graphs are individual.

3.1 Reference measurement: Corneometer

To visualize the range of moisture reached by each subject and make sure that the whole procedure was respected, the data collected by the corneometer are represented for every trial. The corneometer values are expressed from 20 to 120 corresponding to different levels of humidity. The range 20-40 corresponds to a very dry state, 40-60 to a dry state, 60-80 to a medium level of humidity, 80-100 to a wet state, and 100-120 corresponds to a very wet state. About the 15 repetitions, they are separated at each change of normal force during the loading on the MeV2. After 5 trials, the normal force was changing and, since the order was not the same for each subject, it is recalled on each figure, and the droplet of ether or water was applied.

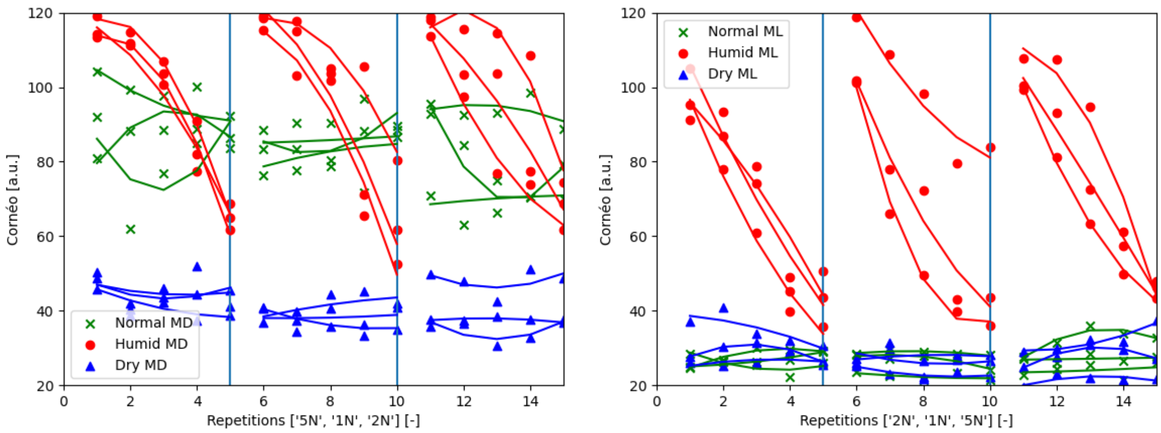

(a) Corneometer values for a subject that starts with a high normal humidity level

(b) Corneometer values for a subject that starts with a high normal humidity level

Figure 3.1: Corneometer data for each trial represented by the different nodes. The different humidity states are represented with different markers: red circles for the 'humid' state, green crosses for the 'normal' state, and blue triangles for the 'dry' state. 3 conditions for each humidity state are represented by the 3 lines. The water or ether is applied after 5 trials, vertical lines.

Figure 3.1 reveals the methodology used during the experiment. The three different levels of moisture described earlier are represented by three different colors. Blue corresponds to a droplet of ether applied on the fingerpad before every 5 repetitions, red is for a condition where the fingerpad is tapped on a wet tissue every 5 repetitions, and green is for the normal humidity state. It was observed that some subjects started with an already low moisture level and thus had trouble reaching values as high as other subjects during the 'humid' state. Similarly, subjects that started with an already high moisture level, could not reach values as low as other subjects even with the droplet of Ether. However, the large panel of subjects allows the research to reach a large range of humidity.

The red curves also described the phenomenon established earlier [25] saying that, when we apply water on the finger's skin, a high moisture level is reached before drying. Indeed, at the end of the five trials, the fingerpad hydration lies in Corneometer values that correspond to wet or very wet skin. It is in opposition to the dry procedure that does not allow a fast rehydration of the skin, and thus the moisture level stays low during the end of the experiment.

3.2 MeV2 measurement: raw data

As said in section 2.2, tangential forces, normal force, and voltage have been recorded with the MeV2 probe. They are all written in a Comma-separated values file unique for each subject. A representation has been made for each condition and each level of humidity. That gives 9 figures for the following conditions: 'Normal' moisture + "Calibration" condition (Figure 3.2a), 'Normal' moisture + "Occlusion" condition (Figure 3.2b), 'Normal' moisture + "Slide" condition (Figure 3.2c), 'Humid' moisture + "Calibration" condition (Figure 3.2d), 'Humid' moisture + "Occlusion" condition (Figure 3.2e), 'Humid' moisture + "Slide" condition (Figure 3.2f), 'Dry' moisture + "Calibration" condition (Figure 3.2g), 'Dry' moisture + "Occlusion" condition (Figure 3.2h), 'Dry' moisture + "Slide" condition (Figure 3.2i). In order to compare each parameter on the same timeline, the MeV2 output, the normal force, and the tangential force appear on the same figure.

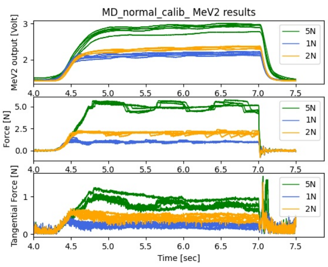

(a) Calibration condition with the normal humidity state

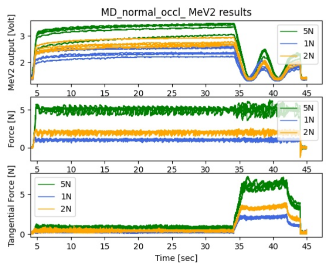

(b) Occlusion condition with the normal humidity state

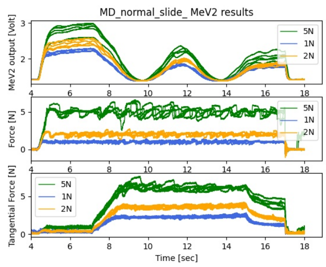

(c) Slide condition with the normal humidity state

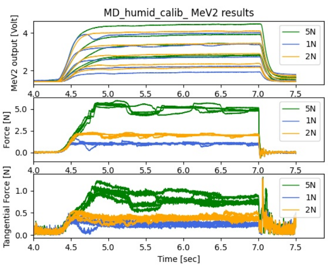

(d) Calibration condition with the high humidity state, water application

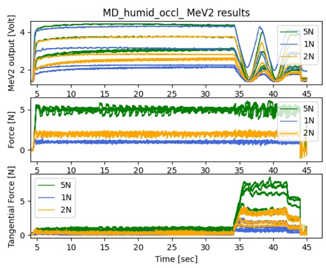

(e) Occlusion condition with the high humidity state, water application

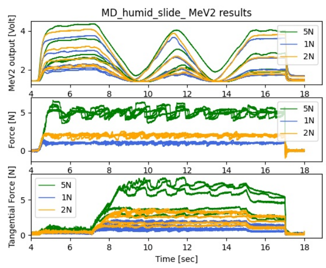

(f) Slide condition with the high humidity state, water application

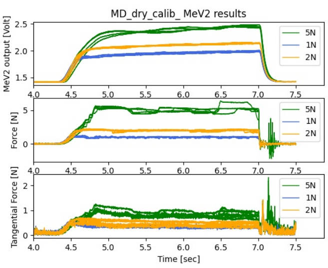

(g) Calibration condition with the low humidity state, ether application

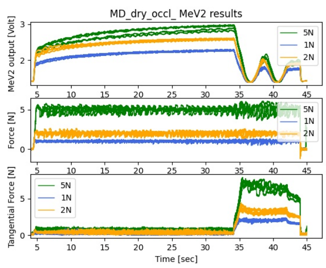

(h) Occlusion condition with the low humidity state, ether application

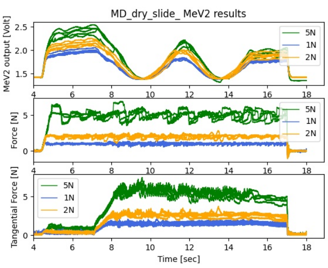

(i) Slide condition with the low humidity state, ether application

Figure 3.2: Raw data output from the MeV2, and the two force/torque sensors. Comparison of the instantaneous current (upper graph), normal force (medium graph), and tangential force (lower graph) through time. The normal load is represented for each graph in green for 5N, in orange for 2N, and in blue for 1N.

3.2.1 Mev2 output

The upper graph in each image of Figure 3.2 illustrates the instantaneous current readings obtained from the MeV2. The initial observation highlights the influence of the applied load force on these values. Specifically, the green lines, representing a normal force of 5N, consistently exhibit higher values than the orange lines, representing 2N, which in turn are higher than the blue lines, corresponding to a load of 1N. This demonstrates a direct correlation between the load force and the recorded current by the MeV2. An ANOVA test comparing the impact of the Normal Force on the Mev2 output rejects the null hypothesis saying that two or more conditions have a similar mean (F=154.2654, pvalue=9.2234e-63). In the case of the humid state, the interpretation is somewhat less straightforward due to the potential interference caused by water application. Immediately after applying water, a droplet may settle on the probe and introduce bias in the outputs. Nevertheless, for the repetitions that follow, the droplet is removed by cleaning the probe, and the humidity level is better controlled.

During the displacement in both the "occlusion" and "slide" conditions, the current comes and goes as the finger reaches the different patches, as depicted in Figure 3.3. The first peak represents the right patch, the second peak corresponds to the middle patch, and the final peak is obtained when the left patch is reached. As the finger moves from one patch to another, the current generally shows a decreasing trend. This decrease is consistently observed because the local maximum on the newly reached patch is consistently lower than the one on the previous patch. This phenomenon can be attributed to two possible factors. Firstly, it is possible that some moisture is deposited on the transparent glass surface, leading to an excess in the recorded current. The presence of moisture could alter the conductivity properties and the efficiency of the transfer of electrical signals. Secondly, another explanation lies in the variations in the contact area between the patch and the finger during the displacement. The skin undergoes deformations as it moves, resulting in differences in the contact area. These variations in contact area can affect the current readings, causing a decrease in the recorded values.

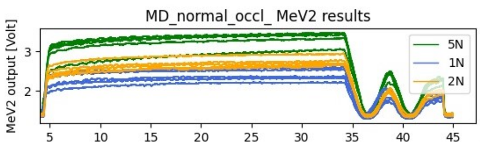

(a) Evolution of MeV2 output in the "occlusion" condition. It is characterized by an increase during the occlusion time on the right patch followed by two other peaks corresponding to the middle and left patches

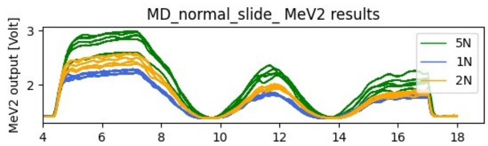

(b) Evolution of MeV2 output in the "slide" condition. It is characterized by three peaks corresponding to the different patches, going from right to left.

Figure 3.3: Focus on the evolution of MeV2 output during sliding induced by the displacement of the robot. The robot is only in motion during the "collusion" and "slide" conditions.

The "occlusion" condition reveals an increase in the current during the prolonged loading phase. To prove this observation, the difference between the last and the first seconds of this phase has been computed for the different levels of humidity (Figure 3.4). The difference between the arithmetic means, computed over one second, of the current has been extracted for the 15 trials of the entire panel of subjects. During the loading phase, the current increases with an average of 0.25 Volt in the 3 conditions with a statistical significance of the impact of the level of humidity on the increase of the current during the loading time (ANOVA test: p-value= 0.01156). Yum et al. proposed that occlusion of sweat within the pores located in the ridges stimulates the plasticization of the skin, resulting in a significant enhancement in friction [27]. Consequently, the observed elevation in current during the prolonged loading phase can be attributed to the occlusion phenomenon. However, previous research observed that the friction was supposed to be maximized and thus, in a humid state, the moisture level should decrease during the occlusion time. No decrease of the current during the static contact is observed.

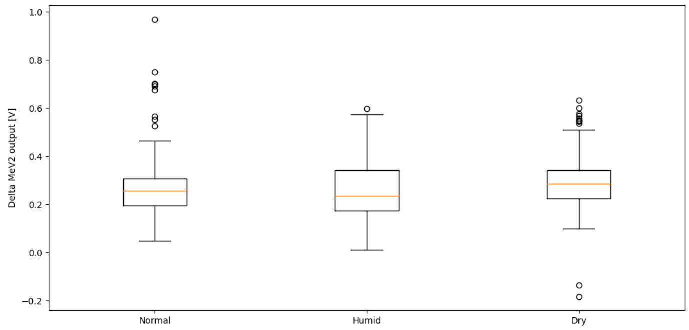

Figure 3.4: Difference of voltage between the first and the last second of the occlusion time for the 3 humidity states (from left to right, 'Normal' state, 'Humid' state, and 'Dry' state). The orange lines represent the median of the sample.

3.2.2 Normal force

The middle graph in each image of Figure 3.2 illustrates the instantaneous normal force obtained from the force sensors. Since one aim of the apparatus is to reach the most constant controlled normal force against the transparent glass, this value was regularly checked during the experiments. The fluctuations increase during the sliding since the finger jumps sometimes when the tangential forces are high.

3.2.3 Tangential force

The lower graph in each image of Figure 3.2 illustrates the instantaneous tangential force obtained from the force sensors. During a static contact, these force values are quasi-null since the robot remains static and thus does not induce any x or y reaction from friction. However, in every condition, a dominant impact of the normal force on the tangential force can be observed. The green curve under loading of 5N remains higher than the orange and blue curves. To validate that observation, the p-value is computed with a one-way ANOVA test. This statistical test compares the mean values of each normal force condition with a null hypothesis being the equality of those means. A value of $p\text{-value} << 0.001$ confirms that the impact of the different normal forces (1N, 2N, 5N) on the tangential force is statistically significant.

At the end of the movement, the graph of tangential force allows us to observe the relaxation phenomenon. Indeed, when the robot begins to move, some tangential stresses appear. When the last patch is found under the subject's index, the robot stops its motion and the fingerpad's skin releases shear stress.

3.2.4 Recapitulative table

The previous values are extracted instantaneously and are time-dependent. To compare the different parameters between the subjects, it was necessary to reduce the noise in those data and also the number of values. A data frame was constructed for each volunteer, comprising the mean values of the different parameters for each trial. In addition to the raw data extracted from the MeV2 and from the force/torque sensors, the Corneometer values are also listed with the corresponding trial. Using the arithmetic means allows us to reduce the data for each parameter to only one and still have an idea of the comportment of the subject.

Condition	Trial	NF[N]	MeV2 [V]	TF[N]	Corneo[a.u.]
normal calib	1	5.01794	2.748895008	0	104.1
normal calib	2	5.03858	2.942189239	0	99.2
normal calib	3	4.87602	2.888051861	0	97.7
normal calib	4	5.04529	2.92851439	0	88.7
normal calib	5	4.85504	2.976466039	0	92.4
normal calib	6	0.99975	2.213073113	0	88.6
normal calib	7	1.01206	2.188823491	0	77.6
normal calib	8	1.00346	2.152018567	0	78.8
normal calib	9	0.98970	2.141852155	0	96.8
normal calib	10	0.99513	2.110196829	0	88.5
normal calib	11	2.00545	2.294623107	0	71
normal calib	12	2.01448	2.353996523	0	63
normal calib	13	1.99757	2.339969774	0	74.9
normal calib	14	1.97240	2.287040256	0	70.7
normal calib	15	2.01885	2.355223867	0	70.1
...					

Table 3.1: Recapitualtive table of every trial for each subject. Columns represent the name of the condition with the humid state used, the trial number corresponding, the MeV2 mean output for the first right patch, the mean tangential force during the displacement (non-null in "Occlusion" and "Slide" conditions), and the Corneometer value after each trial. It has a size of 135x7.

3.3 Calibration of the MeV2

The output of the MeV2 is supposed to reflect the moisture level reached by the fingerpad during contact. In order to validate the MeV2 and calibrate its outputs, we use the Corneometer values as references.

The mean values of the MeV2 output on the first and last patches are compared in figure 3.5. Considering that the Corneometer value is obtained immediately after contact with the last patch, it is more pertinent to calibrate the MeV2 using the values from this last specific patch. However, due to doubts regarding the accuracy of this value based on previous explanations, it was imperative to verify whether the value of the first patch could be utilized. The first right patch is represented in green while the last left patch is represented in red. The difference between the two patches is confirmed and the global trend of the two patches is similar. Since the correctness of the values on the first patch and the shape of the graph is similar between the red and green objects, using the first patch as a reference is appropriate.

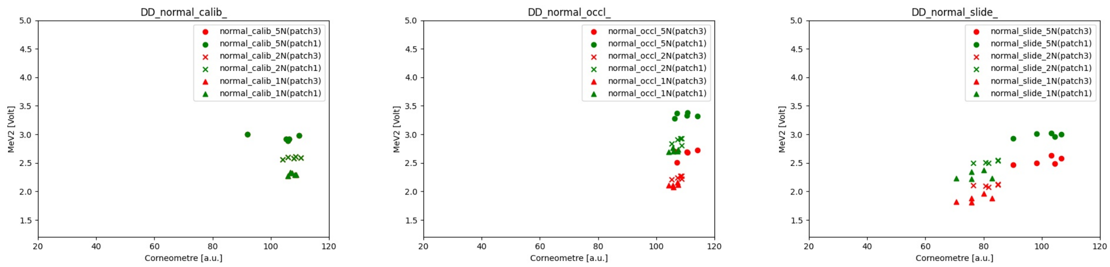

Figure 3.5: Comparison between MeV2 outputs over the first patch (in green) and the last patch (in red) corresponding to the Corneometer values taken after each trial. The three conditions are represented: "Calibration" on the left, "Occlusion" in the middle, and "Slide" on the right. The values of only one subject are shown.

Using the mean MeV2 output values from the right patch, a first representation of the relationship between the Corneometer values and the MeV2 can be shown for one subject in figure 3.6a. The first observation reflects the correlation between high voltage and high Corneometer values. Similarly, low MeV2 values lay in the range of dry contact. However, the normal force seems to impact the correlation between the new and the certified apparatus. Those visualizations can be generalized for the whole panel of participants (Figure 3.6b).

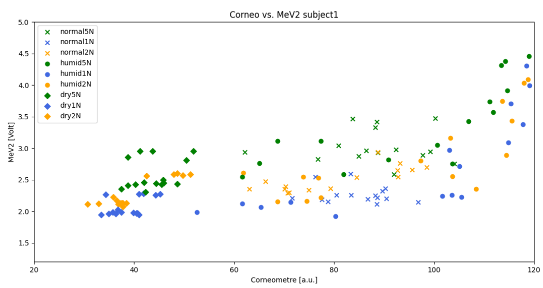

(a) Representation for one subject

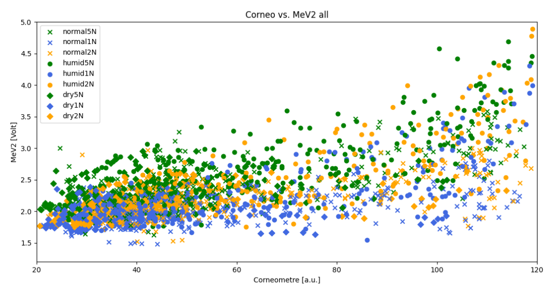

(b) Representation for the 16 subjects

Figure 3.6: $MeV2_{mean}$ over the first patch corresponding to the Corneometer value of the same trial. The different humidity states by 3 markers and different normal forces are represented by 3 colors: crosses for the normal state, points for the humid state, squares for the dry state, green for NF of 5N, orange for NF of 2N, and blue for NF of 1N.

The values obtained during the 'calibration' condition are utilized to calibrate the MeV2. Indeed, this condition reduces the loss of moisture by evaporation or deposit due to the direct use of the corneometer without any sliding during the contact. The only inaccuracy would happen if the water content of the fingerpad, during the 'humid' state, stays on the glass and thus creates a difference between the moisture level on the MeV2 and on the Corneometer. However, it was asked to the subjects not to over-humidify their finger to avoid the creation of an external layer of water.

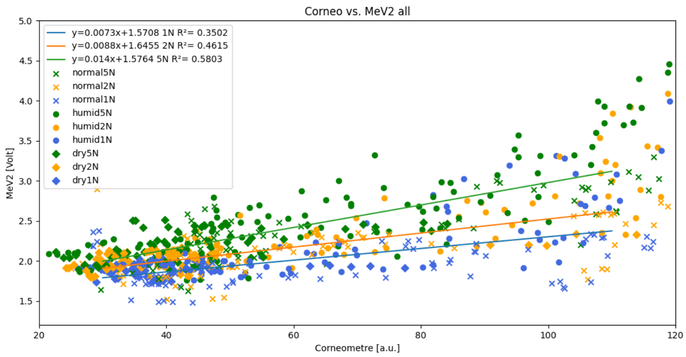

Figure 3.7: $MeV2_{mean}$ over the first patch corresponding to the Corneometer value of the same trial in the "calibration" condition. The three lines represent a linear regression for the three normal forces: blue for 1N, orange for 2N, and green for 5N. The equations of the regressions are used to calibrate the MeV2.

Once the data were plotted, a linear regression of those data for the different load forces was done to estimate the relationship between the MeV2 output and the Corneometer value (Figure 3.7). This linear regression is computed over a smaller interval of 10 to 110[a.u.] taking into account that, below or above that range, the corneometer saturates. The following equations are obtained:

$$y = 0.0073x + 1.5708 \tag{3.1}$$

$$y = 0.0088x + 1.6455 \tag{3.2}$$

$$y = 0.014x + 1.5764 \tag{3.3}$$

where x is the Corneometer value, and y is the MeV2 value obtained by the regression. Equation 3.1 represents the linear regression under a load force of 1N, Equation 3.2 represents values under a load force of 2N, and Equation 3.3 represents values under a load force of 5N. To estimate the correctness of this model, Pearson's correlation coefficients for the 3 linear regressions are computed. The values obtained are:

Condition	R^2	**p-value**
1N	0.3502	1.5736e-19
2N	0.4615	2.1751e-26
5N	0.5803	1.84503e-41

Table 3.2: Pearson's correlation results for the 3 different levels of load force

Those values show a significant correlation between the corneometer and the MeV2 output. The MeV2 output directly represents the moisture level contained in the fingerpad. After introducing the MeV2 values as the y in equations 3.1, 3.2, and

3.3, calibrated MeV2 outputs of 1N, 2N, and 5N can thus be obtained by computing the value of x. We can use those values to analyze the impact of moisture on the following biomechanical properties. The newly calibrated values were compared using Pearson's correlation and a statistically significant correlation was found (R^2=0.4274, p-value<<0.001).

3.4 Impact of moisture on the friction

Adams et al. demonstrated the influence of moisture on friction[28]. Using the MeV2 moisture evaluation and the arithmetic means of tangential over the 90 trials corresponding to the "occlusion" and "slide" conditions, we tried to observe similar results in figure 3.8. The blue makers represent the values under a normal force of 1N, the orange makers represent the values under a normal force of 2N, and the green makers are for the values under a normal force of 5N.

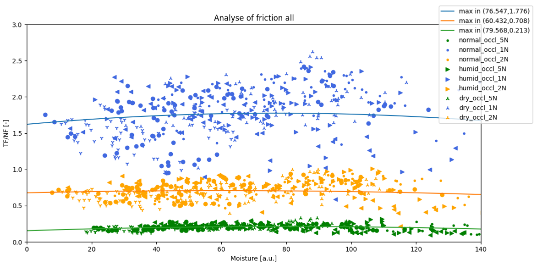

(a) Impact of moisture on friction with the calibrated values of the MeV2.

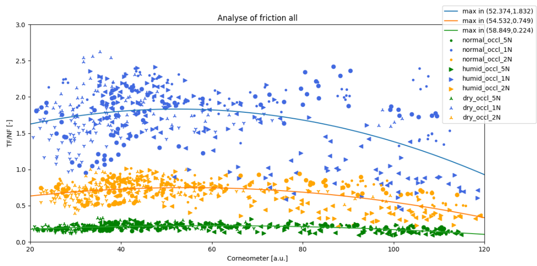

(b) Impact of moisture on friction with the Corneometer values.

Figure 3.8: Friction as a function of the moisture level. The three lines represent the second-degree polynomial approximations for the three levels of normal force: blue for 1N, orange for 2N, and green for 5N. The maxima are written in the graph's legend.

In order to find the relationship that bounds the friction with the tangential force, an approximation of different order is tested. The best fit corresponds to the second-degree approximation following those equations:

$$y_{1N} = -2.596 * 10^{-5}x^2 + 0.004x + 1.622 \tag{3.4}$$

$$y_{2N} = -8.317 * 10^{-6}x^2 + 0.001x + 0.678 \tag{3.5}$$

$$y_{5N} = -9.328 * 10^{-6}x^2 + 0.001475x + 0.155 \tag{3.6}$$

where x correspond to the moisture value and y to the friction. It means that a maximum of friction is reached for a medium value of humidity. Indeed, the maxima are reached between 60 and 80 [a.u.] which corresponds to a regular moisture level. This was also revealed in previous experimentations. The maximum value reached for friction under a normal force of 1N, 2N, and 5N is respectively 1.75, 0.7, and 0.2. There is thus an important decrease in friction due to the load force. In addition, we can observe that the curvature rate decreases with an increasing normal force, meaning that the impact of the moisture on the friction is less important with high load forces.

Since there seems to be an interaction between the three following parameters Normal Force, Moisture level, and Friction, a statistical test is used to determine its relevance. For each value of friction, the load intensity and the humidity level are attributed. The load intensity corresponds to '1N', '2N', or '5N'. The moisture level is determined as follows: less than 50 a.u. correspond to a 'dry' state, more than 90 a.u. corresponds to a 'humid' state, and the in-between is for the 'normal' state.

	df	sum_sq	mean_sq	F	PR(>F)
C(moist)	2.0	2.320166	1.160083	4.937522	7.299851e-03
C(nf)	2.0	307.599914	153.799957	654.600343	1.563836e-200
C(moist):C(nf)	4.0	8.812002	2.203000	9.376367	1.775353e-07
Residual	1377.0	323.529530	0.234952	NaN	NaN

Figure 3.9: Two-way ANOVA test to express the impact of normal force and moisture on friction.

The results from the two-way ANOVA test (Figure 3.9) show that both the Normal Force and the Moisture level have an impact on friction (p-values<<0.05).

3.5 Images measurement: contact area

Images recorded during the experiment allows us to obtain the gross area and the ratio between real area and gross area as explained in section 2.4.1. Since those values are given in pixels per frame, the x-axis can be expressed in second knowing that the frequency is 50 Hz, and the y-axis can be expressed in mm^2 knowing the specifications of the camera (14 µm square pixels). The real area is obtained by multiplying the ratio by the gross area.

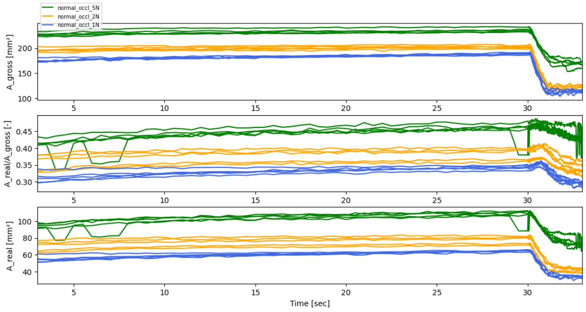

(a) Representation during the "occlusion" condition. Between t=3 and t=30, the contact is static describing an occlusion phenomenon.

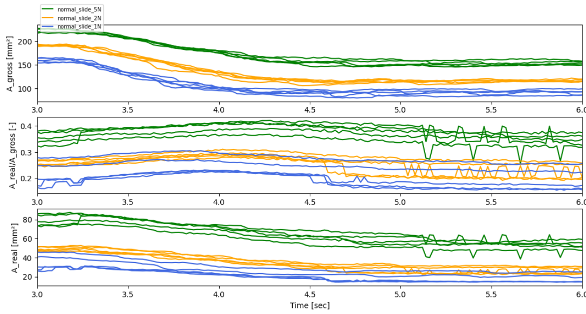

(b) Representation during the "slide" condition. Only the three first seconds of the movement are represented.

Figure 3.10: Comparison of the instantaneous gross area (upper graph), the ratio between the real area and the gross area (medium graph), and the real area (lower graph) through time. The normal load is represented for each graph in green for 5N, in orange for 2N, and in blue for 1N

The prolonged static contact, represented in figure 3.10a, shows that the real area increases during the occlusion phenomenon, getting larger the ratio between the real area and the gross area. The gross area does not vary since the normal force is constant during contact. As soon as the sliding starts, both areas decrease, as observable in figure 3.10b, due to the skin's deformation. With the "slide" condition, a focus on the sliding part shows that the ratio between the two areas remains quite constant even under deformation.

3.5.1 Impact of the normal force

The different load forces are represented by the different colors, there is a direct impact of this force on the areas. This observation has been tested with an ANOVA statistical test and the results show a significant impact of the Normal Force on the contact areas.

Parameter	F	**p-value**
A gross	1433.3	<< 0.001
A real	480.558	2.953e-203
Ratio	163.529	5.176e-71

Table 3.3: ANOVA test to express the impact of Normal Force on 3 different parameters (Gross area, real area, and the ratio between those areas).

Adams et al. found a power law linking the normal force and the contact area as described in equation 1.6 [18]. The coefficients vary with the subject. Using the experimental values for the gross area and the normal forces, we can express the gross area (in mm^2) depending on the normal for one subject.

NF [N]	A_{gross} **[mm^2]**
1	183.15774763779526
2	200.42636627450978
5	233.26334376470587

Table 3.4: Experimental values of the gross area for the different normal forces.

This gives us the following equation:

$$A_{gross} = 183 * (NF)^{0.15} \tag{3.7}$$

3.5.2 Impact of humidity

The MeV2 allows us to compare the instantaneous moisture value with the contact area while a patch is located under the finger. The impact of humidity on the ratio between the real area and the gross area can thus be analyzed but only in the 'occlusion' condition before the start of the motion. From Figure 3.11, a relevant linear correlation between humidity and the real contact area for the different normal forces is observed (p-values of the Pearson's correlation are lower than 0.001), as well as for the ratio of areas. When the moisture level increases, the ratio between the real area and the gross area increases.

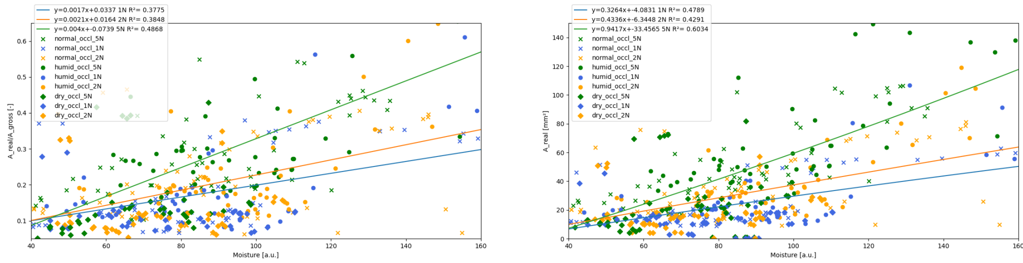

Figure 3.11: Evolution of the real contact area (right) and the ratio of contact areas (left) with moisture. Linear regression for the different levels of NF are represented: green for 5N, orange for 2N, and blue for 1N.

Another parameter seems to have an impact on the relationship between the contact areas and the moisture level. Indeed, the normal force plays a role that we cannot avoid. In order to estimate the dependence of these two independent parameters which are the moisture level and the normal force on the ratio between the contact areas, a two-way ANOVA test is run (Figure 3.12). The normal force is categorized as "1N", "2N", and "5N", while the moisture level is divided as followed: < 50 [a.u.] for a dry state, > 90 [a.u.] for a humid state, and the interval between those values stands for a normal humidity state.

	df	sum_sq	mean_sq	F	PR(>F)
C(nf)	2.0	1.907860	0.953930	191.279469	3.507274e-72
C(Humidity_state)	2.0	1.813716	0.906858	181.840701	4.160704e-69
C(nf):C(Humidity_state)	4.0	0.109109	0.027277	5.469555	2.313793e-04
Residual	1119.0	5.580565	0.004987	NaN	NaN

Figure 3.12: ANOVA test to express the impact of normal force and humidity state on the ratio between the real contact area and the gross contact area.

The statistical test reveals that both normal force and moisture level explain a significant amount of variation in the ratio of contact areas (p values < 0.001).

3.5.3 Impact of friction

The impact of friction can only be analyzed during full slip motion otherwise the tangential forces would be null. In addition, it was observed that the ratio of areas remains constant during the displacement. It was thus decided to represent the variation of the ratio induce by the friction with the mean TF computed earlier (section 3.2.4) and the arithmetic mean of the ratio over each trial. The legend remains the same as previously: green for a normal force of 5N, orange for a normal force of 2N, blue for a normal force of 1N, crosses for the normal state, points for the humid state, and squares for the dry state.

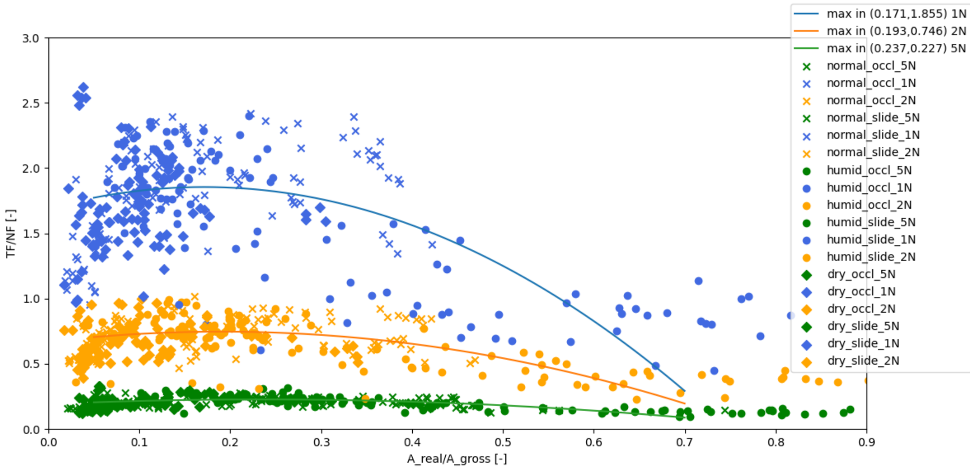

Figure 3.13: Friction as a function of the ratio between the real contact area and the gross contact area. The three lines represent the second-degree polynomial approximations for the three levels of normal force: blue for 1N, orange for 2N, and green for 5N. The maxima are written in the graph's legend.

A bell-shaped curve in figure 3.13 implies the maximization of friction for a certain ratio between the real contact area and the gross contact area. Indeed, a ratio higher than 0.7 is not realistic and means that a layer of water remains on the fingerpad and reduces friction as in Figure 3.14. In addition, every maker higher than this value come from humid condition confirming our supposition. Similarly, values close to 0 reflect a contact too dry to distinguish the contact points. No variation of luminosity can be observed.

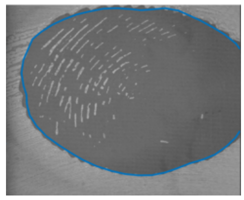

Figure 3.14: Images of a very wet fingerpad resulting in the incapacity to extract a pertinent real area value.

Similar to the impact of moisture on friction, the normal force seems to have an impact on the relationship between contact areas and friction. The maximal friction reached under 1N is higher than for the other normal force. However, this maximum is reached with a higher ratio under 5N. Normal force impacts both, the friction and the contact areas. Statistical tests allow us to look at the impact of individual parameters as well as all together. From p-values in Figure 3.15, the results state that the ratio of contact areas, the normal force, and the humidity state are all significant predictors of the variation in friction of the fingerpad in contact with the glass (p-values $<< 0.001$). There are also significant interaction effects between these three factors which confirm the previous observations.

	df	...	PR(>F)
C(Ratio)	2.0	...	4.248833e-78
C(Normal_Force)	2.0	...	0.000000e+00
C(Humidity)	2.0	...	3.007670e-11
C(Ratio):C(Normal_Force)	4.0	...	2.278775e-34
C(Ratio):C(Humidity)	4.0	...	2.086637e-05
C(Normal_Force):C(Humidity)	4.0	...	1.612710e-06
C(Ratio):C(Normal_Force):C(Humidity)	8.0	...	4.004784e-05
Residual	926.0	...	NaN

Figure 3.15: Three-way ANOVA test to express the impact of the humidity state, the normal force, and the ratio between the real contact area and the gross contact area on friction.

3.6 Images measurement: deformations

The contact area decreases during motion due to deformations. We would like to know how those deformations act under different loading conditions and humidity states. The dataset consisted of instantaneous deformation measurements obtained under various humidity conditions during each trial.

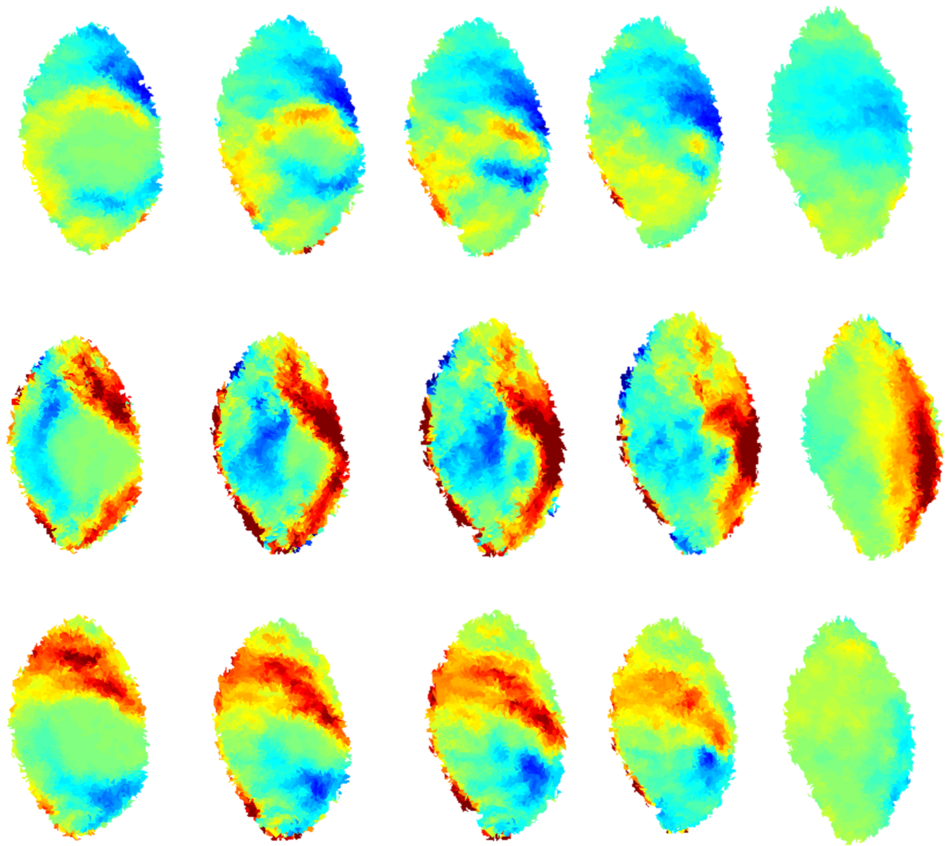

Figure 3.16: Strain evolution for the ulnar displacement over one trial. Each row represents a strain component: first row ϵ_{xx}, second row ϵ_{yy}, and third row ϵ_{xy}. The time scale from left to right corresponds to a displacement of t_1=0.98s, t_2=1.12s, t_3=1.18s, t_4=1.24s, and t_5=1.58s. For a full slip around 1.17s.

From figure 3.16, a progressive strain wave is observed, propagating from the periphery to the center of the contact area. The ulnar displacement induces a proximal displacement of the stuck area. Indeed, the stuck area is located between the compressive and tensile strains. As Delhaye et al. described, in this case, most of the first micro-slips occur at the distal periphery of the contact area and progress proximally later which induces a systematic rotation of the contact area [4].

To investigate the relationship between humidity and fingerpad deformations, a representative numerical value is used to quantify the deformations. This value is the maximal shear stress reached during the displacement as shown in figure 3.17. This value was usually obtained one second after the start of the robot's displacement. The x-axis of the graph represents the number of frames after the start of the motion, knowing that the images were recorded with a frequency of 50 Hz. For the following analysis, the strains will be given in percent.

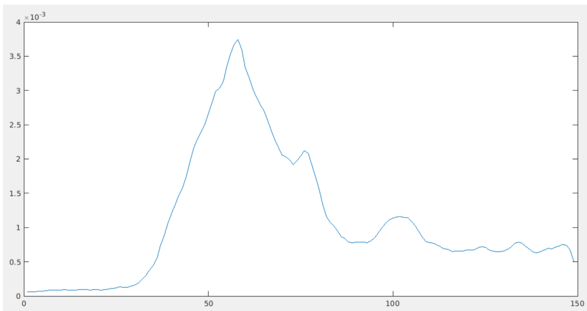

Figure 3.17: Evolution of the maximal shear stress over all the frames corresponding to the first three seconds of the displacement in one trial.

3.6.1 Impact of the normal force

It was previously observed that the normal force has a dominant impact on the biomechanical properties of the fingerpad. It was thus decided to have a look at its impact on deformations before focusing on the humidity. After a comparison of the shear stress under 1N, 2N, and 5N (Figure 3.18), a one-way ANOVA test revealed a non-significant relationship between the normal force and the deformation (F=2.42, pvalue=0.0914). In consequence, changing the normal force of the contact does not influence the deformations.

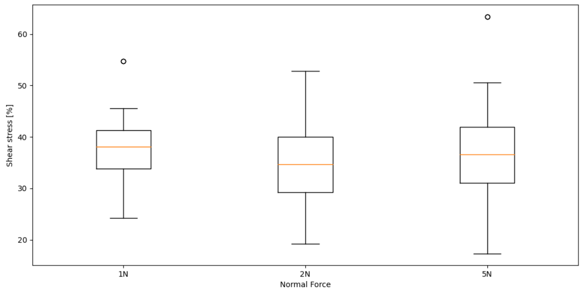

Figure 3.18: Comparison of the maximal shear stress reached under the different normal forces by several subjects. The yellow line represents the median for the different groups.

3.6.2 Impact of humidity

The mean value of Mev2 in the initial patch represents the moisture level achieved by the fingerpad just before the displacement of the robot. This value is compared to the maximum shear stress to investigate the influence of humidity as seen in figure 3.19. To facilitate a comparative analysis of the moisture level, it was decided to differentiate between 'slide' conditions and 'occlusion' conditions. This separation enables the examination of the moisture level attained at the conclusion of prolonged contact and shorter contact instances, considering similar initial humidity conditions.

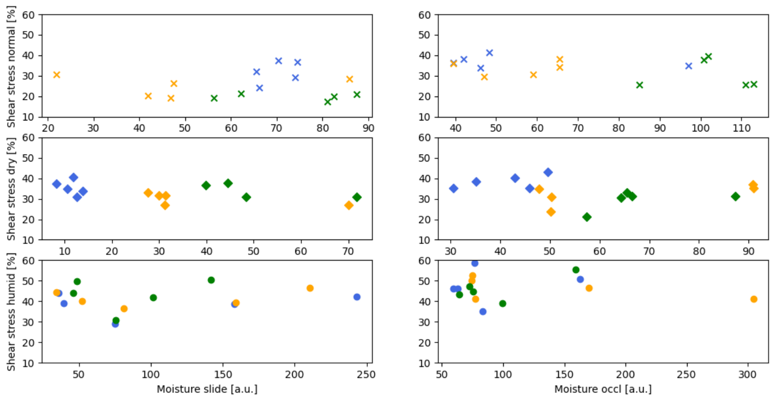

Figure 3.19: Comparison of the maximal shear stress as a function of moisture in the different conditions for one subject. The left column represents the "slide" condition, and the right column represents the "occlusion" condition. The first row shows the normal humidity state, the second row shows the dry state, and the third row shows the humid state.

The first observation is a consequence of the occlusion phenomenon. Indeed, in the 'occlusion' condition, for every humidity state, the range of moisture reached is higher than the one in the 'slide' condition. A long static contact increases the moisture level of the fingerpad.

The impact of humidity on the deformations of the fingerpad was assessed through an analysis of variance (ANOVA), which yielded to a p-value of 0.00755. This finding indicates that there may be statistically significant differences in deformation measurements across different humidity conditions.

3.6.3 Impact of friction

To validate the influence of moisture on deformations, an investigation into the impact of friction was conducted. Given the substantial effect of moisture on friction, any correlation between friction and deformation could potentially imply a relationship with moisture. Consequently, figure 3.20 illustrates the deformations over the different values of friction.

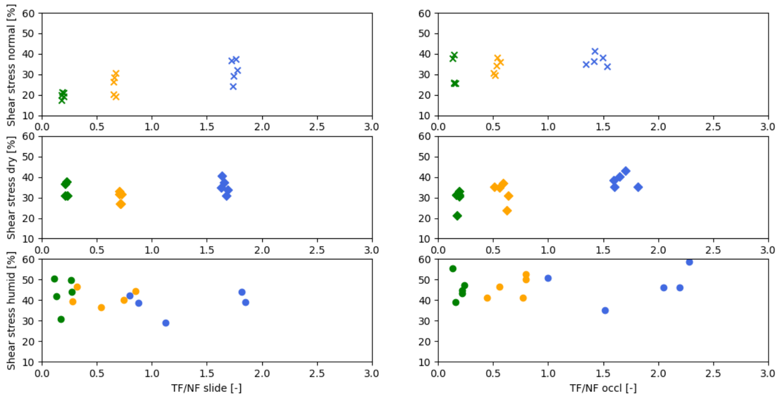

Figure 3.20: Comparison of the maximal shear stress as a function of friction in the different conditions for one subject. The left column represents the "slide" condition, and the right column represents the "occlusion" condition. The first row shows the normal humidity state, the second row shows the dry state, and the third row shows the humid state.

To assess the interdependence of the two independent parameters, namely moisture level and friction, on deformations, a two-way analysis of variance (ANOVA) test was employed. Friction was categorized as high friction (values greater than 2), low friction (values lower than 1), and regular friction (values between these two thresholds). The moisture level was divided as follows: values below 50 [a.u.] denoting a dry state, values exceeding 90 [a.u.] indicating a humid state, and the range between these values representing a normal humidity state.

	df	sum_sq	mean_sq	F	PR(>F)
C(Humidity)	2.0	31.097691	15.548845	0.229096	0.795459
C(Friction)	2.0	333.336969	166.668485	2.455685	0.088363
C(Humidity):C(Friction)	4.0	43.273752	10.818438	0.159398	0.958548
Residual	202.0	13709.833006	67.870460	NaN	NaN

Figure 3.21: Two-way ANOVA test to express the impact of friction and humidity state on the deformations.

The ANOVA test results, represented in figure 3.21, indicate that there is no significant dependence on deformations from either of the two parameters. This implies that humidity alone does not exert any impact on deformations, and similarly, friction does not demonstrate any statistically significant influence on deformations. The interaction between friction and moisture is also not significant in the study of deformations.

Chapter 4

Discussion

Humidity has an important impact on various biomechanical properties of the fingerpad. For a better understanding of object manipulation, it is necessary to take into account the different consequences that a change in humidity can entail. The MeV2 allows us to register any changes in normal force, contact area, and moisture at any time during the experiment.

It was already observed that after prolonged static contact, the fingerpad's moisture level naturally increases[26]. This phenomenon is called occlusion. It is supposed to maximize the coefficient of friction[27]. The protocol used during the experiment includes a long and a short static contact to compare the effect of such a phenomenon.

Effectiveness of the apparatus

The outputs of the MeV2 have a direct correlation with the Corneometer. Linear regressions, specific to the normal forces utilized during the experiment, were computed. Equations 3.1 to 3.3 were used to express the MeV2 output as moisture evaluator values. In further research, a larger range of normal forces could be tried to be able to calibrate the MeV2 for any normal forces. A multiple regression with only three normal forces did not give a relevant result.

In addition, constant cleaning of the glass probe is required when water or other fluid is used since the deposit of a droplet would bias the results. Indeed, the current is favored by the presence of water even if the fingerpad does not touch the probe. The first trials after the water application were all compromised.

Focusing on the images, they give feedback about the contact area and allow us to study the skin's deformations during the robot's motion. Nevertheless, the distinction of the contact area for a dry finger cannot be accurate due to an unclear threshold.

There is no neat visual distinction between contact and no-contact points for dry fingerpads which implies a very difficult manual selection of the gross area. Many were not relevant because of this difficulty. A second light with another inclination could be used to make profit from the ridges in order to create higher contrast. Another solution would be to use a second camera to superpose two images and get the best correlation of it.

Impact of humidity on biomechanical properties

The innovative apparatus enabled us to examine the immediate effects of humidity on various biomechanical parameters of the fingerpad. The protocol employed in our study yielded a wide range of moisture levels by employing ether to achieve very low values and water to reach higher values. It allows us to obtain clear contrast between the different humidity states.

A first observation revealed a clear impact of the normal force on the MeV2 output. This effect was deducted through calibration. To facilitate a more comprehensive interpretation of the humidity's impact, we used normalized values that were independent of the normal force. Nonetheless, it is important to note that the normal force still exerted a notable influence on the tangential forces recorded by the MeV2. High tangential forces are obtained under high normal forces.

Analyzing the obtained images, it becomes apparent that friction can be attributed to two mechanisms: deformation and adhesion, as described by Adams et al [17]. Both of these mechanisms are influenced by the normal force, with the adhesion mechanism that additionally depends on the real contact area. The real contact area experiences a considerable influence from the normal force, leading to an increase in contact area as the normal force increases. An exponential relation links the contact area with the normal force as expressed in equation 3.7. A similar power law is used in Adams et al.'s research.

Moisture plays a significant role in the evolution of the contact area. A direct linear correlation between hydration and the contact area is observed, whereby higher moisture levels result in a larger contact area between the fingerpad and the transparent glass compared to lower moisture levels. This phenomenon can be attributed to the plasticization effect of well-hydrated skin. However, a generalized formula that precisely correlates hydration with contact area has not yet been established.

The computation of friction is also dependent on the tangential force (TF) and normal force (NF), as indicated by equation 1.1. The normal force directly impacts friction, with higher coefficients of friction observed under lower normal forces. It is not the only parameter impacting friction. André et al. discovered that moisture also influences friction, with friction reaching its maximum value at an intermediate moisture level [28]. It was confirmed with the MeV2. When plotting friction as a function of moisture, bell-shaped curves appeared showing the maximization of friction for a moisture level between 60 to 80 a.u. This range corresponds to a normal humidity state. Furthermore, the equations reveal that, at high normal force, the impact of humidity on friction is minimized. Therefore, an interaction exists between friction, humidity, and normal force.

As mentioned earlier, friction theoretically depends on the contact area. Indeed, this relationship is also visible experimentally. Bell-shaped curves revealed a maximization of the friction for a mid-value ratio between the real contact area and the gross area. This observation suggests the presence of a thin layer of water between the fingerpad and the glass at a higher contact area ratio, which would result in lower friction. However, it is important to consider potential inaccuracies in the selection of the gross contact area or during the binarization process used to extract the real contact area. Nevertheless, a clear interaction between friction, moisture, normal force, and contact area exists, although a mathematical expression that precisely describes this relationship has yet to be determined.

In another hand, the study of the deformations does not reveal any relationship with the other biomechanical properties. Strain propagations seem to act the same way under a different normal force as under a different humidity state or a different initial contact area. Only the progression of the strain waves toward the center and the proximal displacement as found by Delhaye et al. [6], that corresponds to an ulnar motion, have also been observed in our experiment.

Occlusion phenomenon

Adelmans et al. stated that, when the hand is in constant contact with a surface, a large amount of sweat builds up[23]. This is the occlusion phenomenon. The protocol included a long static contact highlighting this phenomenon. The 30 seconds of contact revealed a natural increase in the moisture level. It allows the fingerpad to reach higher hydration without the addition of water. Occlusion then prevents the evaporation of moisture from the skin's surface. Such an increase in moisture modifies the friction. However, our experiment reveals that the occlusion phenomenon tends to increase the moisture level even with a high initial hydration state. If the moisture level keeps increasing, friction is first going to be maximized before decreasing. This is not consistent with Yum et al. observations who claimed that friction was always maximized with occlusion.

The prolonged static contact also had an impact on the contact area. Indeed, the real contact area was increasing during the occlusion time. This observation corresponds to the enhancement of the fingerpad's viscous properties and to the plasticization of the skin described by Pasumarty et al. [26]. It would augment the adhesion effect.

Chapter 5

Conclusion

The objective of this master's thesis was to investigate the impact of humidity on the biomechanical properties of the fingerpad with the use of a new probe called MeV2. It was necessary to calibrate the MeV2 before further analyses. Once the calibration was done, a study of the interaction of humidity with the normal force, friction, contact area, and deformations was performed.

Firstly, the instantaneous characteristics of the MeV2 outputs were revealed to be innovative and accurate. By comparison with the Corneometer, the current coming from the MeV2 linearly correlated with the moisture values which gives the possibility to evaluate the moisture level at any time during an experiment. It opened the possibility to observe the full occlusion phenomenon. The calibration was only performed over three normal forces which were 1N, 2N, and 5N, however once a generalized equation of the moisture level as a function of any normal force and the MeV2 output is found, the MeV2 will enlarge the possibilities in this research field that is the object manipulation.

Secondly, the study of humidity revealed to have a significant impact on different biomechanical properties such as friction and contact area. In further research, it is necessary to take that interaction into account knowing that humidity can increase or decrease friction. A generalized model of those interactions still has to be elaborated.

To conclude, the calibration of the MeV2 and the various outcomes of our study confirmed a lot of data in the scientific literature, except for the occlusion phenomenon, for which the research made by Yum et al. is not consistent with our results. This work brings advancement in the research of object manipulation. By submitting further suggestions for future studies on the mechanisms underlying the impact of humidity, our research makes it possible to develop knowledge in this field, which is essential in understanding the way human beings work.

Bibliography

[1] Augurelle A-S. et al. "Importance of Cutaneous Feedback in Maintaining a Secure Grip During Manipulation of Hand-Held Objects". In: *J Neurophysiol* 89 (2003). DOI: https://doi.org/10.1152/jn.00249.2002.

[2] Koris A. "Capillary Force". In: *Encyclopedia of Membranes*. Ed. by Drioli E. and Giorno L. Springer Berlin Heidelberg, 2016, pp. 1–2. ISBN: 978-3-642-40872-4. DOI: https://doi.org/10.1007/978-3-642-40872-4_100-2.

[3] Sankaran A. et al. "Adaptive latent fingerprint segmentation using feature selection and random decision forest classification". In: *Information Fusion* 34 (2017), pp. 1–15. DOI: https://doi.org/10.1016/j.inffus.2016.05.002.

[4] Delhaye B., Lefèvre P., and Thonnard J-L. "Dynamics of fingertip contact during the onset of tangential slip". In: *J. R. Soc. Interface* 11.2014069820140698 (2014). DOI: http://doi.org/10.1098/rsif.2014.0698.

[5] Delhaye B. et al. "Measuring fingerpad deformation during active object manipulation". In: *J Neurophysiol* 126 (2021). DOI: https://doi.org/10.1152/jn.00358.2021.

[6] Delhaye B. et al. "Surface strain measurements of fingertip skin under shearing". In: *J. R. Soc. Interface* 13.20150874 (2016). DOI: http://dx.doi.org/10.1098/rsif.2015.0874.

[7] Rebecca Bevans. "Simple Linear Regression — An Easy Introduction 038; Examples". In: *Scribbr* (Nov. 2022). URL: https://www.scribbr.com/statistics/simple-linear-regression/.

[8] The Editors of Encyclopaedia Britannica. "Coefficient of friction". In: *Encyclopedia Britannica* (2020). URL: https://www.britannica.com/science/coefficient-of-friction.

[9] Wackerly D.D., Mendenhall W., and Scheaffer R.L. *Mathematical Statistics with Applications*. Brooks/Cole, Cengage Learning, 2008. ISBN: 9780495110811.

[10] The MathWorks Inc. *MATLAB version: 9.13.0 (R2022b)*. Natick, Massachusetts, United States, 2022. URL: https://www.mathworks.com.

[11] "Information and Instruction Manual for the Corneometer® CM 825 WL probe". In: *Courage + Khazaka electronic GmbH* (2021).

[12] Fluhr J. et al. "Comparative study of five-instruments measuring stratum corneum hydration (Corneometer CM 820 and CM 825, Skicon 200 Nova DPM 9003, DermaLab)". In: *In vitro. Skin Res. Technol* 5 (1999). DOI: http://dx.doi.org/10.1111/j.1600-0846.1999.tb00126.x.

[13] Betts J.G. et al. *Anatomy and Physiology 2e*. OpenStax, Apr 20, 2022. URL: https://openstax.org/books/anatomy-and-physiology-2e/pages/1-introduction.

[14] Reddy J.N. *An Introduction to Continuum Mechanics, Second Edition*. cambridge university press, 2013. ISBN: 9781107025431.

[15] van Kuilenburg J. "A Mechanistic Approach to Tactile Friction". PhD thesis. Oct. 2013. DOI: 10.3990/1.9789036500340.

[16] van Kuilenburg J., Masen M.A., and van der Heide E. "A review of fingerpad contact mechanics and friction and how this affects tactile perception". In: *Proceedings of the Institution of Mechanical Engineers, Part J: Journal of Engineering Tribology* 229.3 (2015). DOI: https://doi.org/10.1177/1350650113504908.

[17] Adams M.J., Briscoe B.J., and Johnson S.A. "Friction and lubrication of human skin". In: *Tribol Lett* 26.3 (2007). DOI: https://doi.org/10.1007/s11249-007-9206-0.

[18] Adams M.J. et al. "Finger pad friction and its role in grip and touch". In: *J R Soc Interface 10: 20120467* (2013). DOI: https://doi.org/10.1098/rsif.2012.0467.

[19] Boulais N. and Misery L. "Merkel cells". In: *J Am Acad Dermatol* 57 (2007), pp. 147–165. DOI: https://doi.org/10.1016/j.jaad.2007.02.009.

[20] Otsu N. "A Threshold Selection Method from Gray-Level Histograms". In: *IEEE Transactions on Systems, Man, and Cybernetics* 9.1 (1979), pp. 62–66. DOI: 10.1109/TSMC.1979.4310076.

[21] Lefèvre P. "LGBIO1112 : Introduction au génie biomédical". In: *Transparents Biomécanique* (2020).

[22] Bevans R. "Simple Linear Regression — An Easy Introduction Examples". In: *Scribbr* (2022). URL: https://www.scribbr.com/statistics/simple-linear-regression/.

[23] Adelman S., Taylor R.C., and Heglund N.C. "Sweating on paws and palms: what is its function?" In: *American Journal of Physiology* 229.5 (1975). DOI: https://doi.org/10.1152/ajplegacy.1975.229.5.1400.

[24] Bochereau S. et al. "Characterizing and Imaging Gross and Real Finger Contacts under Dynamic Loading". In: *IEEE Transactions on Haptics* 10.4 (2017), pp. 456–465. DOI: 10.1109/TOH.2017.2686849.

[25] Tomlinson S.E. et al. "Understanding the Friction Mechanisms Between the Human Finger and Flat Contacting Surfaces in Moist Conditions". In: *Tribol Lett* 41 (2011). DOI: https://doi.org/10.1007/s11249-010-9709-y.

[26] Pasumarty S.M. et al. "Friction of the Human Finger Pad: Influence of Moisture, Occlusion and Velocity". In: *Tribol Lett* 44 (2011). DOI: https://doi.org/10.1007/s11249-011-9828-0.

[27] Yum S.M. et al. "Fingerprint ridges allow primates to regulate grip". In: *Proc Natl Acad Sci U S A* 117.50 (2020). DOI: https://doi.org/10.1073/pnas.2001055117.

[28] André T., Lefèvre P., and Thonnard J-L. "A continuous measure of fingertip friction during precision grip". In: *J Neurosci Methods* (2009). DOI: https://doi.org/10.1016/j.jneumeth.2009.01.031.

[29] André T. et al. "Effect of skin hydration on the dynamics of fingertip gripping contact". In: *J. R. Soc. Interface* 8.4 (2011). DOI: https://doi.org/10.1098/rsif.2011.0086.

[30] André T. et al. "Moisture Evaluator: a direct measure of fingertip skin hydration during object manipulation". In: *Skin Research and Technology* 14 (2008). DOI: https://doi.org/10.1111/j.1600-0846.2008.00314.x.

[31] Jia Y., Li W., and Li G. "The microstructure and mechanical properties of the fingerpad skin". In: *Journal of the Mechanical Behavior of Biomedical Materials* 87 (2018). DOI: https://doi.org/10.1016/j.jmbbm.2018.07.008.

[32] Yuan Y. and Verma R. "Measuring microelastic properties of stratum corneum". In: *Colloids Surf B Biointerfaces* 48.1 (2006). DOI: https://doi.org/10.1016/j.colsurfb.2005.12.013.

Appendix

Representation of the deformations for multiple subjects

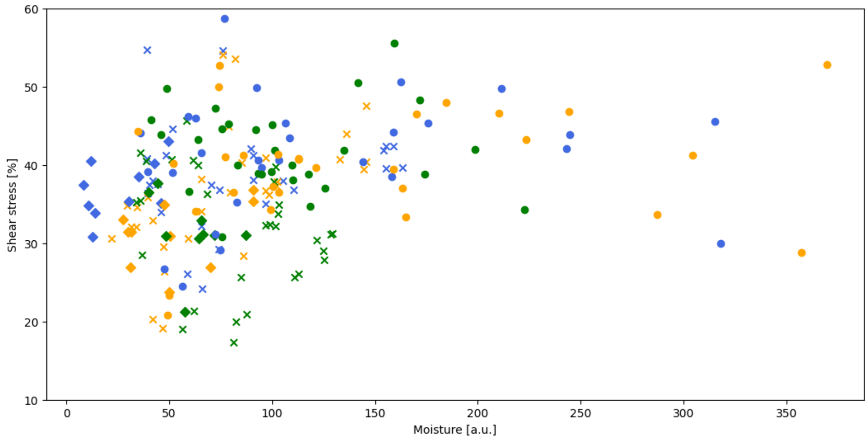

Figure 5.1: Impact of the moisture on the deformations for several subjects.

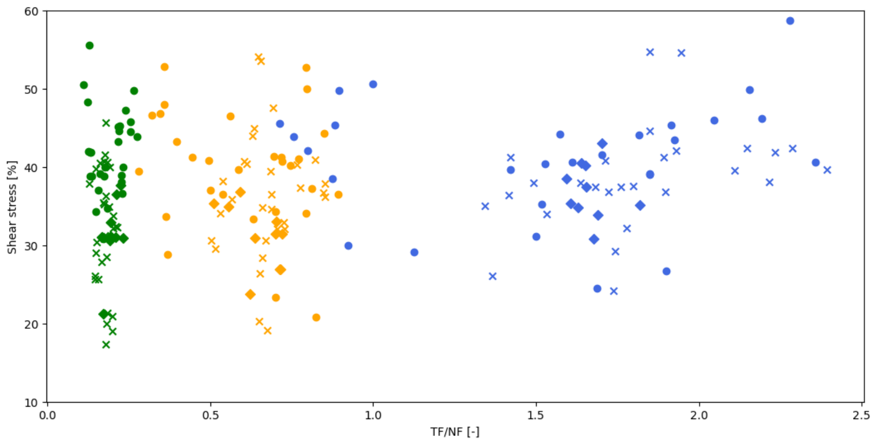

Figure 5.2: Impact of the friction on the deformations for several subjects.

Representation of the contact areas for all the subjects

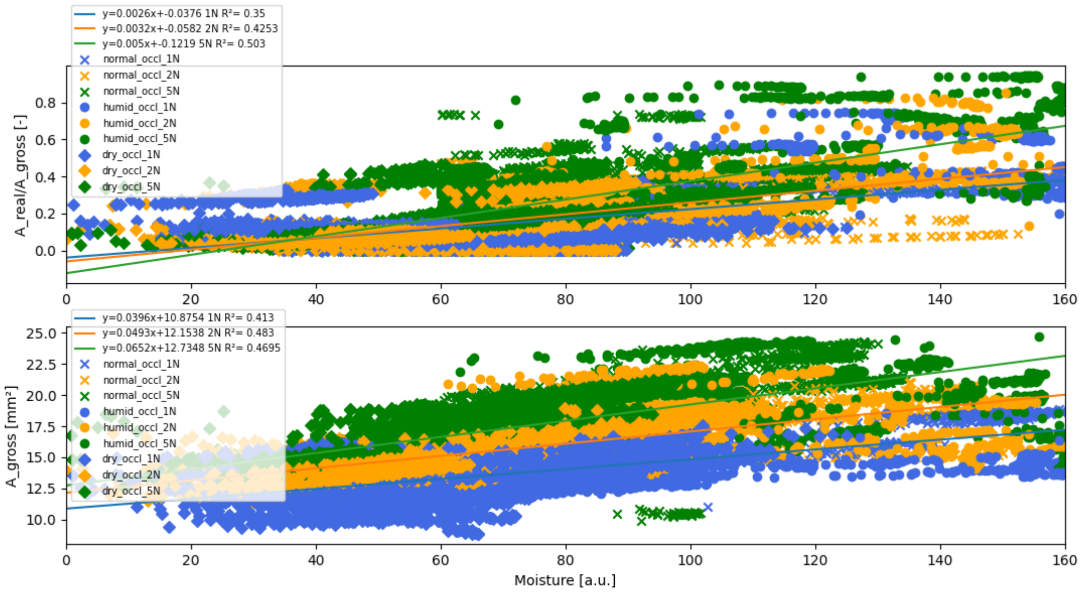

Figure 5.3: Evolution of the gross area and the ratio of contact areas with moisture for several subjects. Linear regression for the different levels of NF are represented: green for 5N, orange for 2N, and blue for 1N.

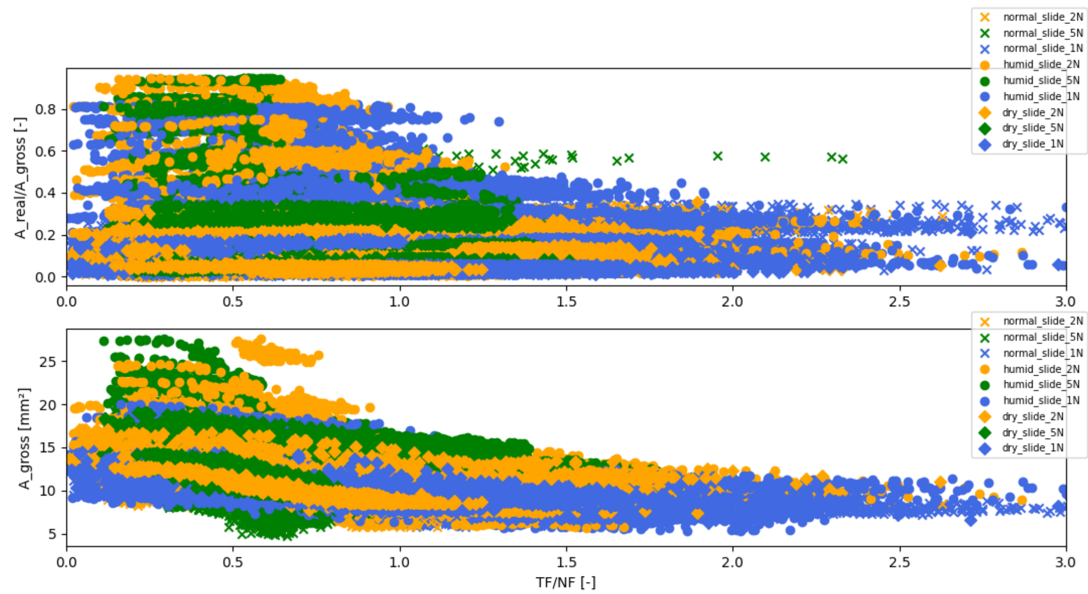

Figure 5.4: Evolution of the gross area and the ratio of contact areas with friction for several subjects. The different levels of NF are represented: green for 5N, orange for 2N, and blue for 1N.

Protocol

1. Calibration

Step	**Position y**	**Position x**	**Time**	**Force**	**Rep**	**Set Camera**
Water/Ether			60000		1x	
Wait	0	0	4000	0	5x	0
Force application	0	0	3000	1	5x	1
Retract	30	20	2000	0	5x	0
Cleaning+Cornéo	30	20	11000	0	5x	0
Water/Ether			30000		1x	
Wait	0	0	4000	0	5x	0
Force application	0	0	3000	2	5x	1
Retract	30	20	2000	0	5x	0
Cleaning+Cornéo	30	20	11000	0	5x	0
Water/Ether			30000		1x	
Wait	0	0	4000	0	5x	0
Force application	0	0	3000	5	5x	1
Retract	30	20	2000	0	5x	0
Cleaning+Cornéo	30	20	11000	0	5x	0
Total time [sec]:			60		5	
additional			120		1	

2. Slide

Step	**Position y**	**Position x**	**Time**	**Force**	**Rep**	**Set Camera**
Water/Ether			60000		1x	
Wait	-22	0	4000	0	5x	0
Force application	-22	0	3000	1	5x	1
Movement	22	0	8800	1	5x	1
Force application	22	0	3000	1	5x	1
Retract	30	20	2000	0	5x	0
Cleaning+Cornéo	30	20	9200	0	5x	0
Water/Ether			30000		1x	
Wait	-22	0	4000	0	5x	0
Force application	-22	0	3000	2	5x	1
Movement	22	0	8800	2	5x	1
Force application	22	0	3000	2	5x	1
Retract	30	20	2000	0	5x	0
Cleaning+Cornéo	30	20	9200	0	5x	0
Water/Ether			30000		1x	
Wait	-22	0	4000	0	5x	0
Force application	-22	0	3000	5	5x	1
Movement	22	0	8800	5	5x	1
Force application	22	0	3000	5	5x	1
Retract	30	20	2000	0	5x	0
Cleaning+Cornéo	30	20	9200	0	5x	0
Total time [sec]:			90		5	
additional			120		1	

3. Occlusion

Step	Position	Position	Time	Force	Rep	Set Camera
Water/Ether			60000		1x	
Wait	-22	0	4000	0	5x	0
Force application	-22	0	30000	1	5x	1
Movement	22	0	8800	1	5x	1
Force application	22	0	3000	1	5x	1
Retract	30	20	2000	0	5x	0
Cleaning+Cornéo	30	20	12200	0	5x	0
Water/Ether			30000		1x	
Wait	-22	0	4000	0	5x	0
Force application	-22	0	30000	2	5x	1
Movement	22	0	8800	2	5x	1
Force application	22	0	3000	2	5x	1
Retract	30	20	2000	0	5x	0
Cleaning+Cornéo	30	20	12200	0	5x	0
Water/Ether			30000		1x	
Wait	-22	0	4000	0	5x	0
Force application	-22	0	30000	5	5x	1
Movement	22	0	8800	5	5x	1
Force application	22	0	3000	5	5x	1
Retract	30	20	2000	0	5x	0
Cleaning+Cornéo	30	20	12200	0	5x	0
Total time [sec]:			180		5	
additional			120		1	
				Normal=	27.5	[min]
				Humid=	33.5	[min]
				Dry=	33.5	[min]
				Total=	1h34min30	

Check list

Before the experiment:

- ☐ On a table: 1 cup with the wet paper, the bottle of ether, 1 cup full of water, the clean towel for the Corneometer.
- ☐ Put a clean towel for the probes on the desk.
- ☐ Turn on the 4 computers: Cameras, Robot, main computer and Corneometer computer with USB connection.
- ☐ Switch on the multiple plugin
- ☐ Give the ethic chart to the subject (+age +left/right-handed +man/woman)
- ☐ Start the program of the cameras, the robot and the Corneometer.
- ☐ Put the protocol on the main computer and name the file of the robot and of the Corneometer.
- ☐ Set the ideal position of the subject's finger.
- ☐ Verify that the camera is under the central probe.
- ☐ Switch on the small light
- ☐ Do the focus of the camera.
- ☐ Set the start position of the robot.
- ☐ Manual trigger the camera and the robot to check if it works.
- ☐ Give the Corneometer to the subject.
- ☐ Show how to use the Corneometer to the person (+erase the data before starting).

- ☐ Clean hands with soap 10 to 15 minutes before

During the experiment:

- ☐ Give the proper name for the file on the Corneometer program.
- ☐ Start the right window before the all the experiment.
- ☐ Start the left window before each protocol at the same time than starting the chronometer.
- ☐ Make sure that the normal force, and the cameras work well.
- ☐ Clean the probe after each repetition.
- ☐ Save the Corneometer data after each series (15 values)
- ☐ Change the files names after each protocol.

- ☐ Humidify/Dry for one minute (or 30sec) just before starting. (Before each 5 rep)
- ☐ Take a Corneometer measurement after each repetition.
- ☐ Clean the Corneometer.
- ☐ Make sure NOT to move and to relax the hand.
- ☐ Do NOT touch anything with the finger that is analyzed.

Full recapitulative table for one subject

Condition	Trial	NF[N]	MeV2 right[V]	MeV2 left[V]	TF[N]	Corneo[a.u.]
normal_calib_	1	5.01794	2.748895008	NaN	0	104.1
normal_calib_	2	5.038587	2.942189239	NaN	0	99.2
normal_calib_	3	4.876024	2.888051861	NaN	0	97.7
normal_calib_	4	5.045298	2.92851439	NaN	0	88.7
normal_calib_	5	4.855048	2.976466039	NaN	0	92.4
normal_calib_	6	0.999756	2.213073113	NaN	0	88.6
normal_calib_	7	1.012066	2.188823491	NaN	0	77.6
normal_calib_	8	1.003469	2.152018567	NaN	0	78.8
normal_calib_	9	0.989708	2.141852155	NaN	0	96.8
normal_calib_	10	0.99513	2.110196829	NaN	0	88.5
normal_calib_	11	2.005458	2.294623107	NaN	0	71
normal_calib_	12	2.014489	2.353996523	NaN	0	63
normal_calib_	13	1.997576	2.339969774	NaN	0	74.9
normal_calib_	14	1.972405	2.287040256	NaN	0	70.7
normal_calib_	15	2.018858	2.355223867	NaN	0	70.1
normal_occl_	1	4.991894	3.042125726	2.048060729	1.258323	80.9
normal_occl_	2	4.983859	3.325604872	2.268759543	1.219505	88.2
normal_occl_	3	5.034582	3.417252755	2.234607682	1.143171	88.5
normal_occl_	4	5.050818	3.47656109	2.189960244	1.160362	100.2
normal_occl_	5	5.103646	3.465802599	2.199160345	1.22678	83.7
normal_occl_	6	1.005973	2.541380255	1.916272817	2.106917	76.3
normal_occl_	7	0.986892	2.588902761	1.915856631	2.177959	83.3
normal_occl_	8	1.007235	2.364297673	1.797675998	2.031831	90.3
normal_occl_	9	0.990976	2.210259725	1.692322013	2.117613	71.6
normal_occl_	10	1.000222	2.324318063	1.752119942	2.102439	89.7
normal_occl_	11	2.014779	2.654967318	1.830767053	1.60091	95.6
normal_occl_	12	1.982736	2.646053814	1.916616548	1.669512	92.7
normal_occl_	13	1.989675	2.764501276	1.963787533	1.687344	93.2
normal_occl_	14	1.998905	2.694337903	1.957136918	1.689011	98.5
normal_occl_	15	2.00087	2.933029736	1.924422119	1.668475	88.7
normal_slide_	1	5.050136	2.581409172	2.048199379	1.191388	92
normal_slide_	2	4.882599	2.93661991	2.230431966	1.197776	62.1
normal_slide_	3	5.078202	2.824223542	1.899737944	1.273409	76.8
normal_slide_	4	4.9638	2.872819527	2.020007411	1.230842	84.9
normal_slide_	5	5.09564	2.962128042	2.103953038	1.163972	86.4
normal_slide_	6	0.998686	2.260091506	1.865132379	2.153518	83.4
normal_slide_	7	0.987215	2.203244224	1.780735086	2.332534	90.5
normal_slide_	8	0.994578	2.259605554	1.835127912	2.328745	80.5
normal_slide_	9	1.008441	2.251918462	1.800061565	2.309386	88.2
normal_slide_	10	0.998967	2.193740357	1.762122782	2.416454	86.7
normal_slide_	11	1.973575	2.547888383	1.854792942	1.766873	92.8
normal_slide_	12	2.039987	2.536435167	1.891741283	1.692489	84.5
normal_slide_	13	2.002745	2.471185073	1.887373513	1.835727	66.3

normal_slide_	14	2.033693	2.392776942	1.839497004	1.887341	70.3
normal_slide_	15	2.001867	2.357922302	1.801035078	1.889231	79.3
humid_calib_	1	4.972705	4.457750597	NaN	0	119
humid_calib_	2	5.031547	3.910262086	NaN	0	114.7
humid_calib_	3	5.042939	3.422422842	NaN	0	106.9
humid_calib_	4	4.959226	2.816941247	NaN	0	90.9
humid_calib_	5	4.981251	2.760493024	NaN	0	65.1
humid_calib_	6	1.001548	3.99038468	NaN	0	119.1
humid_calib_	7	1.002819	3.373482748	NaN	0	117.8
humid_calib_	8	1.002101	2.711070872	NaN	0	105.1
humid_calib_	9	0.99895	2.223812784	NaN	0	105.5
humid_calib_	10	1.007803	1.919004058	NaN	0	80.3
humid_calib_	11	1.987426	4.0898796	NaN	0	118.8
humid_calib_	12	1.987975	3.430477364	NaN	0	115.6
humid_calib_	13	1.999146	2.885272227	NaN	0	114.5
humid_calib_	14	1.976748	2.353852041	NaN	0	108.4
humid_calib_	15	2.004774	2.163563315	NaN	0	74.5
humid_occl_	1	5.036827	4.376338975	3.842731378	0.651815	114.3
humid_occl_	2	5.088424	3.736754269	2.813630912	0.722685	111.1
humid_occl_	3	5.063633	3.051021055	2.158190375	1.199971	100.6
humid_occl_	4	4.980779	3.10909654	1.971131151	1.420595	77.4
humid_occl_	5	4.890596	3.110118772	1.970493623	1.542996	68.7
humid_occl_	6	0.99809	4.305295729	4.084720637	0.60708	118.5
humid_occl_	7	1.006594	3.090011201	2.899587492	0.708081	114.9
humid_occl_	8	0.992491	2.242976808	2.078349723	1.151833	101.7
humid_occl_	9	0.997917	2.14825539	1.801326255	1.851201	71.3
humid_occl_	10	1.006671	2.117315197	1.742740692	1.9316	61.6
humid_occl_	11	1.991121	3.747407943	3.322932008	0.683517	113.6
humid_occl_	12	1.994145	2.799966551	2.329579633	0.944473	97.3
humid_occl_	13	2.022042	2.53155564	1.857873582	1.494027	76.9
humid_occl_	14	2.022518	2.548222071	1.866608811	1.616498	73.8
humid_occl_	15	1.975618	2.611826347	1.797642249	1.741465	61.8
humid_slide_	1	4.943434	4.314321814	3.981580687	0.596253	113.4
humid_slide_	2	5.016591	3.567821141	2.83312487	0.738011	111.8
humid_slide_	3	5.098134	2.75077286	2.002911924	1.158072	103.7
humid_slide_	4	5.124011	2.581837629	1.916070499	1.326131	81.9
humid_slide_	5	5.109612	2.544004103	1.891055054	1.416622	61.6
humid_slide_	6	0.99034	3.707739385	3.611263958	0.690331	115.4
humid_slide_	7	1.011802	2.966308047	2.603258283	0.88929	103.1
humid_slide_	8	0.982028	2.258485662	2.006465447	1.35909	103.6
humid_slide_	9	1.001265	2.064993683	1.726482659	1.773683	65.4
humid_slide_	10	0.98254	1.985589632	1.716310902	1.958645	52.6
humid_slide_	11	2.010244	4.034188075	3.801043904	0.652001	118
humid_slide_	12	2.001303	3.157634427	2.636322962	0.873055	103.3

humid_slide_	13	1.984051	2.555482641	1.907237417	1.312994	103.7
humid_slide_	14	1.90368	2.213892063	1.77777493	1.673133	77.4
humid_slide_	15	2.006688	2.150464329	1.780391281	1.656872	68.7
dry_calib_	1	5.384811	2.429301048	NaN	0	48.6
dry_calib_	2	5.094132	2.421665918	NaN	0	40.3
dry_calib_	3	4.971077	2.445877877	NaN	0	45.9
dry_calib_	4	5.009654	2.44002422	NaN	0	44.4
dry_calib_	5	4.998026	2.428656358	NaN	0	45.5
dry_calib_	6	1.019294	1.972815572	NaN	0	40.7
dry_calib_	7	0.998591	1.987148717	NaN	0	37.4
dry_calib_	8	0.992505	1.988707501	NaN	0	35.7
dry_calib_	9	0.995686	1.961522392	NaN	0	36.3
dry_calib_	10	1.003263	1.96235469	NaN	0	34.9
dry_calib_	11	1.977078	2.129395224	NaN	0	37.7
dry_calib_	12	2.015094	2.127426472	NaN	0	37.3
dry_calib_	13	2.008104	2.132828633	NaN	0	38.4
dry_calib_	14	1.966908	2.132313153	NaN	0	37.6
dry_calib_	15	1.994871	2.115507136	NaN	0	36.8
dry_occl_	1	4.913755	2.805820809	1.964792184	1.203515	50.4
dry_occl_	2	4.914188	2.855096153	1.942839825	1.311376	38.7
dry_occl_	3	5.075057	2.956065671	1.912570292	1.359073	43.7
dry_occl_	4	4.926521	2.956282159	1.863230941	1.417518	51.9
dry_occl_	5	4.940378	2.949694217	1.88465808	1.34626	41.2
dry_occl_	6	1.033016	2.268865745	1.742734857	2.006953	41
dry_occl_	7	0.997703	2.266389304	1.723366054	2.077765	34.3
dry_occl_	8	1.005845	2.255250825	1.757962594	1.956169	44.3
dry_occl_	9	0.993423	2.270073927	1.765993424	1.966521	45.2
dry_occl_	10	0.99199	2.282177284	1.7639724	1.986711	41.9
dry_occl_	11	2.00576	2.565909079	1.89061955	1.572245	49.7
dry_occl_	12	1.966704	2.588035434	1.862235373	1.715926	47.9
dry_occl_	13	2.011038	2.563099258	1.87283937	1.729423	42.5
dry_occl_	14	1.994611	2.583542529	1.910100984	1.56834	51.3
dry_occl_	15	2.000242	2.598132433	1.897259747	1.450615	48.6
dry_slide_	1	4.988348	2.496212449	2.016709307	0.969814	45.8
dry_slide_	2	5.083724	2.452893384	1.975718142	1.083362	42
dry_slide_	3	5.143008	2.305161576	1.852228591	1.048362	42.3
dry_slide_	4	5.00242	2.349847987	1.928674072	1.105498	37.4
dry_slide_	5	5.005057	2.412257412	1.960601503	1.124137	38.8
dry_slide_	6	1.00001	2.026961094	1.770946084	1.317624	36.7
dry_slide_	7	1.010741	1.979417804	1.769748375	1.455151	39.9
dry_slide_	8	0.999629	1.968612516	1.785082733	1.589296	40.5
dry_slide_	9	0.996776	1.948404575	1.755622154	1.775026	33.4
dry_slide_	10	0.977833	1.941920518	1.7779712	1.583206	41
dry_slide_	11	2.054098	2.221412313	1.97558099	1.066947	35.8

dry_slide_	12	2.000211	2.168412647	1.810517994	1.282013	36.5
dry_slide_	13	1.962427	2.112475229	1.924749521	1.306962	30.7
dry_slide_	14	2.002194	2.117874196	1.895605421	1.357663	32.9
dry_slide_	15	1.992453	2.07669937	1.870215637	1.427187	37.7

UNIVERSITÉ CATHOLIQUE DE LOUVAIN
École polytechnique de Louvain
Rue Archimède, 1 bte L6.11.01, 1348 Louvain-la-Neuve, Belgique | **www.uclouvain.be/epl**